Xiong *et al. Chem. Synth.* **2025**, *5*, 50
DOI: 10.20517/cs.2024.118

Chemical Synthesis

Review

Open Access

Insight on reaction pathways of photocatalytic methane conversion

Yizhe Xiong, Jiahong Liu*, Yiou Wang*

Advanced Research Institute of Multidisciplinary Sciences, Beijing Institute of Technology, Beijing 102488, China.

***Correspondence to:** Jiahong Liu, Prof. Yiou Wang, Advanced Research Institute of Multidisciplinary Sciences, Beijing Institute of Technology, No. 8 Liangxiang East Road, Fangshan District, Beijing 102488, China. E-mail: 3120246349@bit.edu.cn; yiou.wang@bit.edu.cn

How to cite this article: Xiong, Y.; Liu, J.; Wang, Y. Insight on reaction pathways of photocatalytic methane conversion. *Chem. Synth.* **2025**, *5*, 50. https://dx.doi.org/10.20517/cs.2024.118

Received: 30 Aug 2024 **First Decision:** 30 Oct 2024 **Revised:** 8 Nov 2024 **Accepted:** 18 Nov 2024 **Published:** 15 May 2025

Academic Editor: Jun Xu **Copy Editor:** Pei-Yun Wang **Production Editor:** Pei-Yun Wang

Abstract

Methane, one of the primary components of natural gas, is an excellent carbon and hydrogen source with low cost and natural abundance. It serves as an ideal feedstock for the production of high-value-added chemicals and fuels. However, its symmetrical tetrahedral structure presents intrinsic challenges for activation and conversion under mild conditions. Unlike the traditional high-temperature processes of methane reforming (700-1,100 °C) used in industry, the photocatalytic conversion of methane into high-value chemicals under mild conditions has attracted significant attention recently. Such a nature-mimicking approach leads to energy savings, reduces conversion costs, and decreases carbon emissions. However, current research on photocatalytic methane conversion is still far from scaling up, with diverse reaction mechanisms across different reaction systems, and there is a lack of a unified summary regarding the underlying mechanisms. Therefore, it is crucial to summarize various reported mechanisms and pathways, which are essential for guiding the design and optimization of catalysts and reaction systems. Herein, we review the most likely conversion pathways and common methods for photocatalytic methane conversion in different systems. This review categorizes the reaction mechanisms according to four common pathways in photocatalytic methane conversion: partial oxidation, coupling (including oxidative and non-oxidative coupling), functionalization, and reforming. Finally, it offers perspectives on the outlook of photocatalytic methane conversion from the angles of mechanistic research, catalyst design, and practical applications, providing insights into the fundamental aspects of this field.

Keywords: Photocatalysis, methane conversion, mechanism, pathway

INTRODUCTION

With the declining reserve of crude oil and the predicted substantial reserve of methane hydrate and shale gas, there is an increasing need to utilize methane instead of oil as a building block for chemical synthesis in the coming decades[1,2]. However, owing to the inert nature of methane arising from a symmetric tetrahedral structure with a low electron and proton affinity and low polarizability, it is still challenging to convert methane to high-value-added chemicals or high-energy-density fuel at moderate temperatures. Many methods of direct methane conversion have been exploited, including thermocatalytic, electrocatalytic, and photocatalytic. Compared to thermal and electricity, light is directly sourced from nature and operates under mild conditions, leading to a greener and cleaner process. Although light energy is often less intense than thermal and electrical processes for activation, resulting in lower methane conversion yields compared to thermal and electrocatalytic methods, photocatalysis offers more excellent tunability, enhancing product selectivity, which is also highly compelling[3]. In contrast to the enormous heat and electricity energy consumption process, photocatalysis generates charge carriers that activate methane and substantially reduce the activation energy of chemical reactions under mild conditions. This process even allows uphill reactions and overcomes the conventional thermodynamic barrier at room temperatures[4]. Additionally, due to the mild nature of light-driven activation of C–H bonds, photocatalysis is effective in suppressing over-oxidation, thereby preventing coke deposition and significantly enhancing product selectivity. Therefore, photocatalysis is a promising method for C–H bond activation in the conversion of methane. Compared with other catalytic conversion methods, it is evident that the photocatalytic process is a light, energy-saving, and green process that has the potential to reduce emissions and mitigate the greenhouse effect, accompanied by obtaining high value-added chemicals. From an economic point of view, the cost of the photocatalytic process is mainly concentrated in the reaction equipment and catalyst. The design of the reaction system is related to the cost and difficulty of expanding the catalytic system. In addition, the preparation and lifetime of the catalyst are directly related to the cost. At this stage, the photocatalytic methane conversion system would be industrializable when the cost of the system is lower than the value of products for a certain length of time. To achieve this, cost reduction is intuitive, but increasing output by increasing the rate and selectivity of product production and solar conversion efficiency is the key[3]. Therefore, the design of catalysts with higher performance, long life, and low cost and the development of scalable reactors and reaction systems are essential to achieve this production and performance goal. The reaction principles and reaction pathways are key research fundamentals in this regard, although when the system is expanded, catalyst considerations also need to address different problems such as photon transfer limitation, mass transfer limitation, oxygen deficiency, and lack of reaction pathway control[5].

From a reaction mechanism perspective, photocatalysts with appropriate redox potentials are crucial for the conversion of methane, as illustrated in Figure 1A. As for methane, the redox potentials of typical oxidations are E (CH_4/CO_2) = 0.17 V, E (CH_4/CO) = 0.32 V and E ($CH_4/•CH_3$) = 0.83 V *vs.* standard hydrogen electrode (SHE)[6-8]. When the valance band (VB) potential of the semiconductor photocatalyst is more positive than the potential, the photogenerated holes in the valence band thermodynamically can drive the activation of methane. Furthermore, the oxidation of CH_4 also can be initiated by radicals that attack the C–H bond of CH_4[9], commonly including superoxide radicals, hydroperoxyl radicals, and hydroxyl radicals [E ($O_2/•O_2^-$) = -0.33 V, E ($O_2/•OOH$) = -0.05 V, E ($H_2O/•OH$) = 2.30 V, E ($H_2O_2/•OH$) = 1.07 V][10,11]; the thermodynamic potential of the photocatalyst also need to meet specific conditions to drive the process. Therefore, commonly used photocatalysts for methane conversion, such as ZnO, TiO_2, and $SrTiO_3$, possess relatively wide band gaps to thermodynamically facilitate the activation of methane and the generation of reactive species. In addition to the complete oxidation of methane, an appropriate thermodynamic potential of the valence band can effectively mitigate over-oxidation, thereby enhancing the selectivity for intermediate high-value chemicals[12].

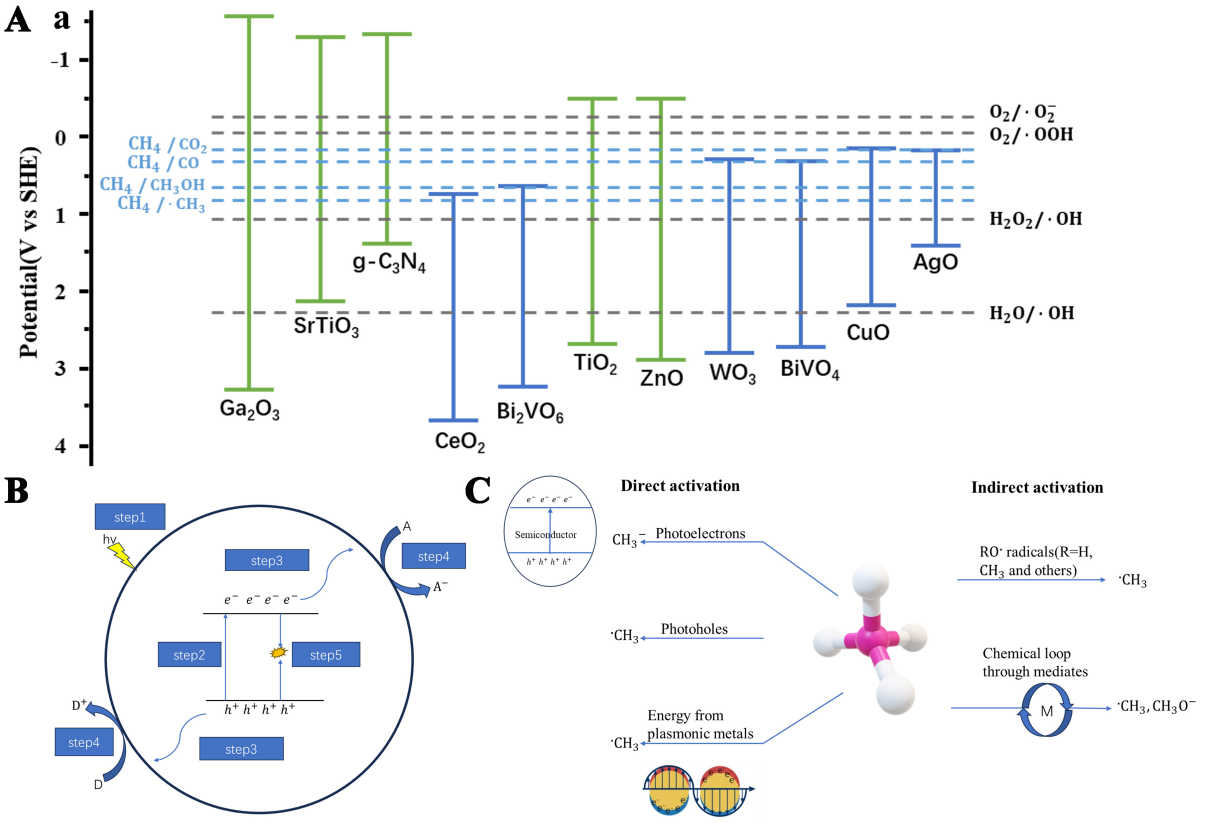

Figure 1. (A) Illustration of the band structures of commonly used semiconductors and the redox potentials of diverse reactants. Reproduced with permission from Ref[9]. Copyright 2021, Wiley-VCH; (B) The principle of photocatalysis involves illumination (step 1), excitation of electrons from the valence band to the conduction band (step 2), charge separation and transportation to the reaction sites (step 3), surface reactions (step 4) and charge recombination on the surface (step 5). A, electron acceptor; D, electron donor; (C) Methane can be activated by different mechanisms photocatalytically. Reproduced with permission from Ref[4]. Copyright 2022, Springer Nature.

In terms of the process, methane conversion is similar to other photocatalytic reactions [Figure 1B]. Upon irradiation with light of an appropriate wavelength, electrons in the valence band of the photocatalyst are excited to the conduction band, leaving behind oxidative holes in the valence band. Some of these charge carriers recombine, while others migrate to the catalyst surface to participate in redox reactions[13]. In this process, the separation of electron-hole pairs is crucial, and common methods to promote this separation include constructing heterojunctions[14], creating built-in electric fields[8], or using co-catalysts[15]. In principle, the C–H bonds in methane can be activated directly by photogenerated charge carriers or by the reactive intermediate radicals produced. Besides, high-energy charge carriers from plasmonics or radical chain reactions also contribute to this activation[16,17]. This article primarily discusses the mechanisms and reaction pathways of the two preceding activation methods [Figure 1C]. The wavelengths of light involved in this review mainly lie in the range from ultraviolet (UV) to visible region, together with some specific examples of methane conversion driven by infrared light and gamma rays.

In recent years, we have witnessed rapid development in photocatalytic methane conversion, which mainly includes four routes: oxidation (including partial oxidation and complete oxidation), coupling (including non-oxidative coupling and oxidative coupling), functionalization, and reforming (including dry reforming and steam reforming). The partial oxidation usually generates C1 oxygenates as target products, such as methanol and formaldehyde. While the non-oxidative coupling produces polycarbonic hydrocarbons, the

oxidative coupling leads to various products, including ethane, ethylene, glycol, *etc*. The functionalization of methane results in halo-methane, borylated-methane, nitrated-methane, *etc*., which holds significant importance in organic synthesis reactions. The dry and steam reforming mainly produces synth gas. With the emergence of this field, numerous reviews on photocatalytic methane conversion have been published, covering topics such as photocatalyst reviews[4,9,18], reactor design reviews[4,19], and reviews of reaction systems[9,20]. However, there remains a lack of summarized pathways and mechanisms for common methane conversion reactions, which are crucial for the design and optimization of these processes. This review comprehensively summarizes and generalizes the universal reaction mechanisms and processes of four main types of reactions for photocatalytic methane conversion. We have also examined the reaction pathways in various systems, compared the latest research advancements across different systems, and provided a critical assessment of the research frontiers and highlights. Finally, we identified the key challenges in photocatalytic methane conversion and offered suggestions for future research, aiming to provide valuable insights for ongoing studies in the field.

PHOTOCATALYTIC METHANE CONVERSION

Total oxidation of methane

Oxidation of methane includes complete and partial oxidation. In terms of product value, total oxidation reactions need to be suppressed, as the chemicals produced are of higher value produced by partial oxidation, as given in

$$CH_4 + 2O_2 \xrightarrow{h\nu} CO_2 + 2H_2O \quad (1)$$

However, the complete oxidation of methane via photocatalysis appears to offer unique advantages in mitigating the greenhouse effect due to traditional combustion methods being ineffective for the oxidation of low concentrations of methane present in the atmosphere[21]. Photocatalytic methane to an equivalent molar amount of carbon dioxide helps alleviate this issue, given that methane is a significantly more potent greenhouse gas and the global warming potential of methane is 29.8 times greater than that of carbon dioxide over a 100-year time horizon according to the IPCC AR6 assessment[3].

For complete oxidation, the oxidation potential of the photocatalyst needs to be more positive to facilitate the complete oxidation of methane thermodynamically. Therefore, commonly used photocatalysts include wide bandgap materials such as ZnO[15], $SrTiO_3$[6], and Ga_2O_3[22], which necessitate the use of UV light as the typical light source. A pioneering study[15] demonstrated the complete oxidation of methane using Ag-loaded ZnO nanoparticles, benefiting from the surface plasmon resonance of silver, which enhances the photocatalytic oxidation of methane [Figure 2A]. This system exhibits robust capabilities for oxidizing low concentrations of methane in both fixed-bed mode [Figure 2B] and flow-gas mode [Figure 2C].

Partial oxidation of methane

The direct partial oxidation of methane primarily aims to selectively produce high-value chemicals such as methanol, formaldehyde, and formic acid. In this process, due to the inert nature of C–H bonds, the reactive radical species required for methane activation typically exhibit high oxidative potential. However, the partial oxidation products (e.g., methanol) often show higher reactivity than methane itself, making them highly susceptible to further oxidation, which will significantly reduce selectivity to a target product. Therefore, the key to this process lies in controlling the reaction pathways mediated by oxidative radicals to enhance selectivity while simultaneously improving conversion rates of methane. Common oxidative radical species involved in the partial oxidation of methane are •OH, •OOH, and $\bullet O_2^-$. These radicals can participate in the reaction separately, and •OH can also participate in the reaction with the other two. The

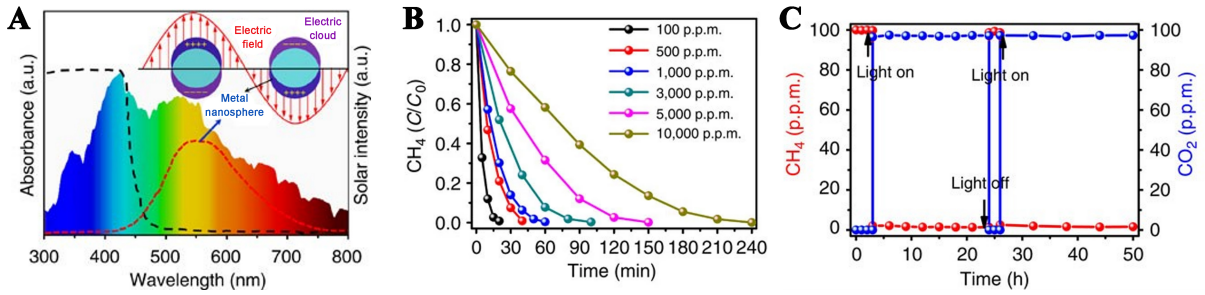

Figure 2. (A) Decorated metallic nanostructures may act as both a co-catalyst and a light-harvesting medium; (B) Time evolution of the methane photooxidation in the fixed-bed mode under full arc illumination with various initial CH_4 concentrations; (C) Methane photooxidation activity under full arc illumination and a flow-gas mode with a gas flow rate of 25 mL·min^{-1}. Reproduced with permission from Ref[15]. Copyright 2016, Springer Nature.

mechanism of the reaction pathway will be introduced according to the key oxidative radicals [Figure 3].

Partial oxidation reactions mainly mediated by •OH

Similar to water oxidation, the oxidation of methane in an aqueous solution is mediated via hydroxyl radicals (•OH), a highly reactive species and one of the most potent oxidizing agents with high oxidation potential (approximately +2.8 V *vs.* SHE) for activation of the C–H bond in methane. •OH can be generated through three primary pathways: oxidation, reduction, and homolytic cleavage of hydrogen peroxide (H_2O_2). In the reduction pathway, •OH is primarily formed by the combination of oxygen with hydrogen radical •H originating from the reduction of the proton by conduction band electrons, as given in

$$O_2 + 2H^+ + 2e^- \xrightarrow{cat} 2\cdot OH \quad (2)$$

These protons are typically derived from water, making water and oxygen common reaction conditions for this mechanism. However, when the thermodynamic potential of the photocatalyst's valence band exceeds 2.73 V (*vs.* SHE), such as Ga_2O_3 and $BiVO_4$ [Figure 1A], OH radicals can also be directly generated from the oxidation of water by holes through one-electron process, as given in[3]

$$H_2O + h^+ \xrightarrow{cat} \cdot OH + H^+ \quad (3)$$

Simultaneously, the protons produced in the reaction can combine with valence band electrons to form H atoms, which subsequently react with oxygen to generate OH radicals [Equation (2)].

Using water as a source of hydroxyl radicals is a common approach in the partial oxidation of methane[23-25], as water is the most abundant and non-toxic reagent. Additionally, by controlling the amount of water, the concentration of radicals can be regulated, directly managing the oxidation process and reducing the occurrence of over-oxidation. As shown in Figure 4A[26], hydroxyl radicals for methane oxidation were generated using biconical $BiVO_4$ as a photocatalyst through direct water oxidation by photogenerated holes. Due to the efficient extraction of photoexcited holes from surfaces with intermediate reactivity for oxidation, the selectivity for methanol exceeded 85% while achieving a production rate of 134 μmol/g/h [Figure 4B and C].

The homolytic cleavage of hydrogen peroxide is another method for generating hydroxyl radicals (•OH). It typically employs metals or metal ions (e.g., Fe[27], W[28], Co[29]) as homolytic catalysts, as given in

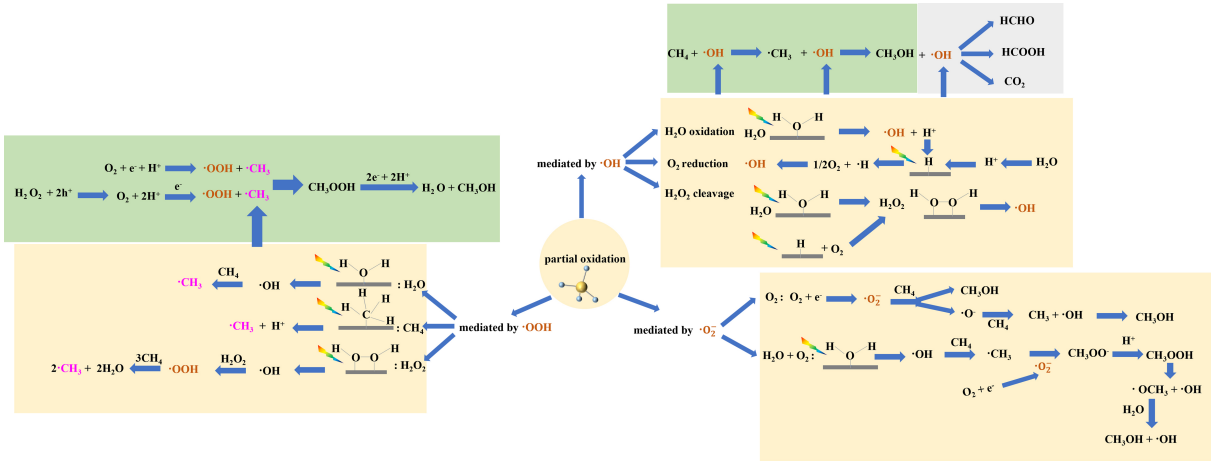

Figure 3. Scheme of the reaction pathways for photocatalytic partial oxidation of methane. To avoid ambiguity and highlight the critical active species within the reaction pathways, some by-products and stoichiometric coefficients are not shown.

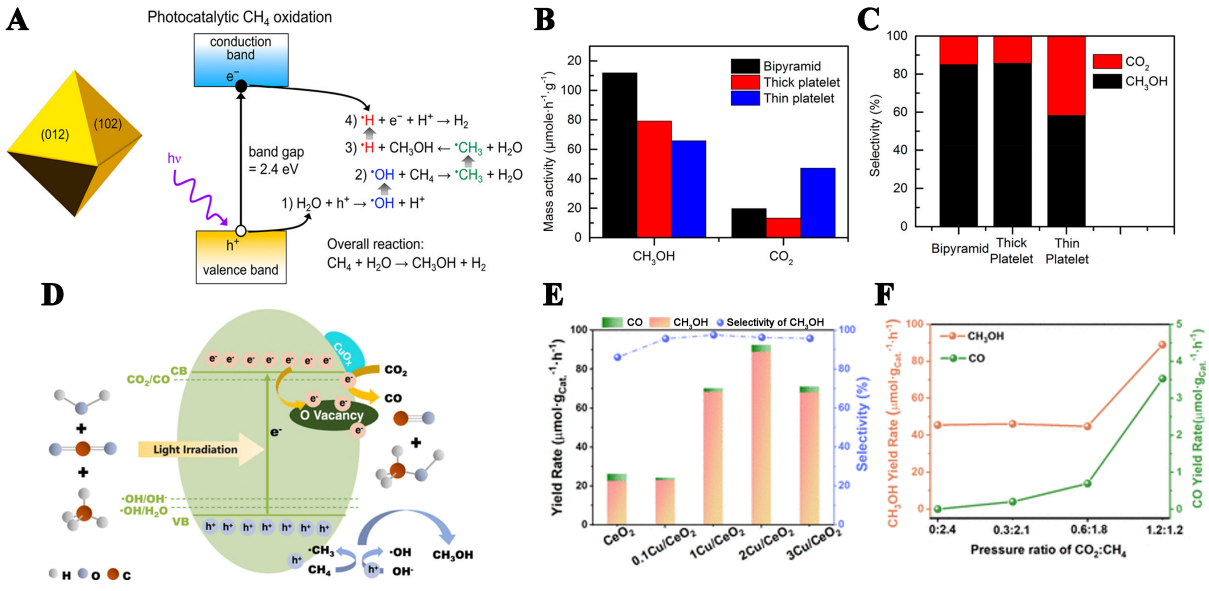

Figure 4. (A) Structure of the biconical $BiVO_4$ photocatalyst and the methane conversion process mediated by hydroxyl radicals generated through direct water oxidation; (B) along with its effects on the selectivity for methanol and carbon dioxide and (C) the corresponding yield. Reproduced with permission from Ref[26]. Copyright 2018, American Chemical Society; (D) Methane conversion process mediated by hydroxyl radicals generated through direct water oxidation assisted by carbon dioxide as a mild oxidant; (E) selectivity and yield of methanol, and (F) the influence of different carbon dioxide concentrations on methanol yield and selectivity. Reproduced with permission from Ref[30]. Copyright 2023, American Chemical Society.

$$M^{n+} + m\,e^- \xrightarrow{cat} M^{(n-n)+} \tag{4}$$

$$M^{(n-m)+} + m\,H_2O_2 \xrightarrow{cat} M^{n+} + m\cdot OH + m\,OH^- \tag{5}$$

Hydrogen peroxide can be introduced directly into the reaction system or generated via water oxidization, as given in

$$2\,h^+ + 2\,H_2O \xrightarrow{cat} H_2O_2 + 2\,H^+ \quad (6)$$

As a summary, •OH can be produced by H_2O, O_2, and H_2O_2. It mainly follows the mechanisms given in Equations (2-6). The •OH is usually used to realize the conversion from methane to methanol, as determined by

$$\cdot OH + CH_4 \xrightarrow{cat} \cdot CH_3 + H_2O \quad (7)$$

$$\cdot OH + \cdot CH_3 \xrightarrow{cat} CH_3OH \quad (8)$$

Because hydroxyl radicals are strong oxidants, current research aims to raise the selectivity of CH_3OH while maintaining a high production rate, where over-oxidation is almost inevitable. This is mainly done by

$$\cdot OH + CH_3OH \rightarrow \cdot CH_2OH + H_2O \quad (9)$$

$$\cdot OH + \cdot CH_2OH \rightarrow HCHO + H_2O \quad (10)$$

$$\cdot OH + HCHO \rightarrow \cdot CHO + H_2O \quad (11)$$

$$\cdot OH + \cdot CHO \rightarrow HCOOH \quad (12)$$

$$\cdot OH + HCOOH \rightarrow \cdot COOH + H_2O \quad (13)$$

$$\cdot OH + \cdot COOH \rightarrow CO_2 + H_2O \quad (14)$$

Therefore, in hydroxyl radical-mediated partial oxidation of methane, the key to improving methanol selectivity lies in controlling the concentration of hydroxyl radicals. High concentrations of hydroxyl radicals can easily over-oxidize the methanol product, reducing selectivity, while low concentrations may be insufficient to activate methane fully, significantly limiting methanol yield. Therefore, precise regulation of hydroxyl radicals is crucial in this process. Various methods have been employed, such as controlling exposed crystal facets to generate hydroxyl radicals at appropriate concentrations selectively or using mild radical inhibitors, such as nitrates, to prevent the over-oxidation of methane to improve the selectivity of methanol significantly. Another strategy is to adjust the step of direct water oxidation by holes to produce hydroxyl radicals, which can be assisted by using mild oxidants that combine with electrons to modulate the concentration of hydroxyl radicals, thereby enhancing selectivity. As shown in Figure 4D[30], carbon dioxide, a mild oxidant, can assist in the oxidation of water by holes to generate hydroxyl radicals at an optimal concentration. The weak oxidizing nature of carbon dioxide, combined with conduction band electrons, facilitates the hole-driven water oxidation process, achieving a high methanol selectivity of 96.2% and a high production rate of 88.9 $\mu mol \cdot g^{-1} \cdot h^{-1}$ [Figure 4E]. With the increase in carbon dioxide concentration, both the yield and selectivity of methanol improved, demonstrating the auxiliary role of mild oxidants such as carbon dioxide [Figure 4F].

Hydroxyl radicals can also mediate the oxidative coupling reactions, which will be discussed in the below sections.

Partial oxidation reactions mediated by •OOH

•OOH is another key reactive species involved in the partial oxidation of methane, typically originating from the combination of oxygen and protons, as given in

$$O_2 + H^+ + e^- \rightarrow \cdot OOH \quad (15)$$

During methane conversion, the combination of methyl radicals with •OOH readily forms CH_3OOH through

$$\cdot CH_3 + \cdot OOH \rightarrow CH_3OOH \quad (16)$$

which can then react with protons and electrons to produce methanol and water, thus achieving high selectivity for methanol, as given in

$$CH_3OOH + 2H^+ + 2e^- \rightarrow CH_3OH + H_2O \quad (17)$$

Methyl radicals can be generated directly using photocatalysts with valence band potentials higher than that required for methane dehydrogenation[31,32], or through synergistic oxidation (water[33-36] and hydrogen peroxide[37-41]) with other oxidants to activate the C–H bond.

Due to the thermodynamic oxidation potential of OOH (1.44 V *vs.* SHE), which is lower than that of the hydroxyl radical (2.8 V *vs.* SHE), controlling selectivity toward methanol in the partial oxidation of methane is more feasible from the perspective of avoiding over-oxidation. However, this is at odds with the more positive oxidative potential of hydroxyl radicals required for methane activation. Consequently, the reaction pathway for methane in this process still needs to be carefully regulated to prevent excessive oxidation. One approach is to use water as the source of hydroxyl radicals and oxygen as the source of hydroperoxyl radicals, with both radicals participating in the reaction. The reaction mechanism still follows Equations (15-17) and

$$CH_4 + h^+ \rightarrow \cdot CH_3 + H^+ \quad (18)$$

but the methyl radical is generated through the activation of methane by hydroxyl radicals produced from the oxidation of water [Equation (3)]. For example, in 2021, Cai *et al.* employed Au–Pd/TiO_2 as a photocatalyst to oxidize methane in the presence of water and oxygen [Figure 5A][42]. In this process, hydroxyl radicals from water dehydrogenate methane, while the hydroperoxyl radicals [Figure 5B] formed from the reduction of oxygen combine with methyl radicals to form CH_3OOH [Equation (16)]. Thanks to the mild oxidation effect of oxygen, a high methanol yield of 8.6 mmol·g^{-1} and a selectivity of 42.8% for methanol were achieved [Figure 5C].

Another proposed method is to directly activate methane using a photocatalyst with a valence band thermodynamic potential more positive than that required for methane dehydrogenation [E (CH_4/•CH_3) = 0.83 V] [Figure 1A], thus generating methyl radicals without relying on hydroxyl radicals [Figure 5D] [Equation (18)].

For instance, depositing CoO_x on an Au-TiO_2 photocatalyst can consume photogenerated holes, preventing the formation of •OH and selectively producing methanol [Figure 5E] via the previously mentioned universal mechanism [Equations (15-17)] [Figure 5F][31]. This approach has also been effective with other catalysts [Figure 5E], significantly enhancing methanol selectivity to break through 95%[31]. Despite various approaches proposed to avoid over-oxidation by hydroxyl radicals, most studies continue to use reaction systems where water and oxygen coexist[33-36]. These studies generally adhere to the reaction mechanism mentioned above while employing other strategies to enhance methanol selectivity, such as adjusting

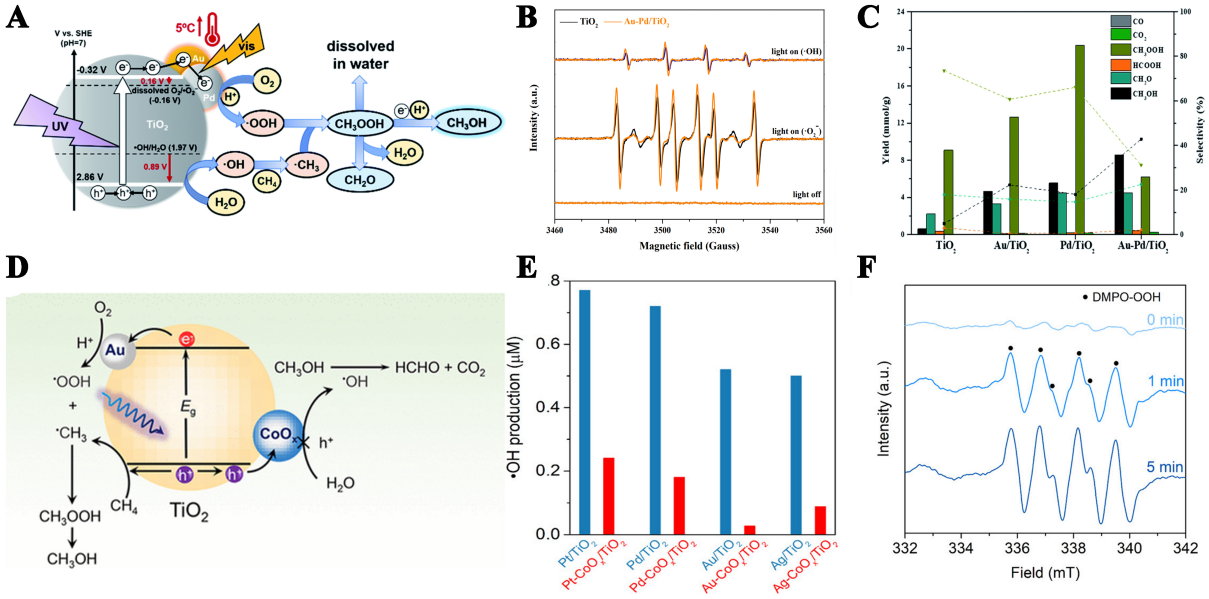

Figure 5. (A) Reaction mechanism of photocatalytic methane conversion over Au–Pd/TiO_2; (B) EPR spectra of the catalyst suspension with DMPO as the spin probe; (C) Photocatalytic methane oxidation over TiO_2, Au/TiO_2, Pd/TiO_2, and Au–Pd/TiO_2 under UV-visible light irradiation (5 mg catalyst, 30 mL water, 3.0 MPa CH_4, 1.0 MPa O_2, 1 h reaction). Reproduced with permission from Ref[42]. Copyright 2021, Royal Society of Chemistry; (D) Proposed reaction process of photocatalytic CH_4 oxidation on Au/TiO_2 and Au-CoO_x/TiO_2 using O_2 as the oxidant; (E) •OH production of photocatalysts in 1 mM coumarin aqueous solution; (F) *In situ* EPR spectra of Au-CoO_x/TiO_2 in CH_3OH aqueous solution dissolving O_2 with different light illumination times. Reproduced with permission from Ref[31]. Copyright 2020, American Chemical Society. EPR: Electron paramagnetic resonance; DMPO: 5,5-dimethyl-1-pyrroline N-oxide; UV: ultraviolet.

catalyst structures, regulating the adsorption of species at active sites, and using appropriate oxidation inhibitors.

In the partial oxidation of methane mediated by hydroperoxyl radicals, another reaction pathway, besides those occurring in water-based environments, involves the use of hydrogen peroxide. Similar to water, hydrogen peroxide, in combination with conduction band electrons from the photocatalyst, generates hydroxyl radicals by

$$H_2O_2 + e^- \rightarrow \cdot OH + OH^- \quad (19)$$

However, these hydroxyl radicals not only oxidize methane by abstracting hydrogen but also react with hydrogen peroxide to produce essential hydroperoxyl radicals through

$$H_2O_2 + \cdot OH \rightarrow \cdot OOH + H_2O \quad (20)$$

which facilitate the formation of CH_3OOH from methyl radicals [Equation (16)]. Subsequently, as previously discussed, methanol is selectively produced via this mechanism [Equation (17)]. Hydrogen peroxide is more reactive than water, leading to a higher concentration of radicals under comparable conditions. Consequently, the use of hydrogen peroxide in the partial oxidation of methane enhances the methanol production rate, albeit with a reduction in methanol selectivity. Nevertheless, hydrogen peroxide remains an effective reaction medium for the efficient conversion of methane and is widely used in numerous studies.

Depending on the adsorption modes of methane on the active sites, two C–H bond dissociation mechanisms, namely homolytic and heterolytic cleavage, are recognized in methane activation. A recent computational study reveals that heterolytic cleavage is the dominant C–H bond activation pathway for all mixed metal oxide complexes of the form $[M1M2]^{2+}$ (M1 and M2 = Mn, Fe, Co, Ni, Cu, and Zn), with the exception of pure copper[43]. In other words, the design of catalysts plays a more critical role than the oxidant systems as long as the catalyst undergoes the heterolytic activation of methane.

Partial oxidation reactions mediated by $\bullet O_2^-$

Oxygen is a commonly used oxidant for the partial oxidation of methane. However, due to its electrophilic nature, oxygen readily combines with conduction band electrons during photocatalysis, as given in

$$O_2 + e^- \rightarrow \cdot O_2^- \tag{21}$$

Under neutral conditions, the electrode potential for this reaction is -0.16 V (*vs.* SHE). Consequently, when oxygen is used as an oxidant, the inevitable formation of superoxide anion radicals occurs. This leads to a third category of oxidation reactions, primarily mediated by superoxide anion radicals in methane conversion.

According to recent research advancements, this reaction can be classified into two main types: one involving the absence of water[41,44,45] and the other involving its presence. In the absence of the water reaction, methane and oxygen can be mixed in a specific ratio as the reaction gas, with the reaction process primarily following the mechanism outlined below. Initially, oxygen is reduced by photogenerated electrons to form superoxide anion radicals. Then, $\bullet O_2^-$ attacked CH_4 and initiated the breaking of the CH_3–H and the O–O bond together, as given in

$$CH_4 + \cdot O_2^- \rightarrow CH_3OH + \cdot O^- \tag{22}$$

The generating active O radicals further lowered the energy barriers by

$$CH_4 + \cdot O^- \rightarrow \cdot OH + \cdot CH_3 + e^- \tag{23}$$

which produced CH_3OH, resulting in the efficient and selective conversion of CH_4 to CH_3OH, as given in

$$\cdot OH + \cdot CH_3 \rightarrow CH_3OH \tag{24}$$

A direct example of this approach can be seen in a 2021 study[44], where oxygen was used as an oxidant to convert methane to methanol efficiently under anhydrous conditions. The researchers cleverly exploited the oxygen vacancies in the photocatalyst material to facilitate the formation of active oxygen radicals. The reaction mechanism followed the previously given steps [Equations (21-24)], as illustrated in Figure 6A. The *in situ* electron paramagnetic resonance (EPR) spectroscopy revealed that the presence of oxygen vacancies significantly increased the concentration of superoxide anion radicals [Figure 6B], which are crucial in the reaction as they directly oxidize methane and play a key role in enhancing methanol selectivity [Equations (22 and 23)].

In another scenario, the oxidation process involves water, where the mechanism is similar to other water-involved radical-mediated reactions. Valence band holes oxidize water to generate highly oxidative hydroxyl

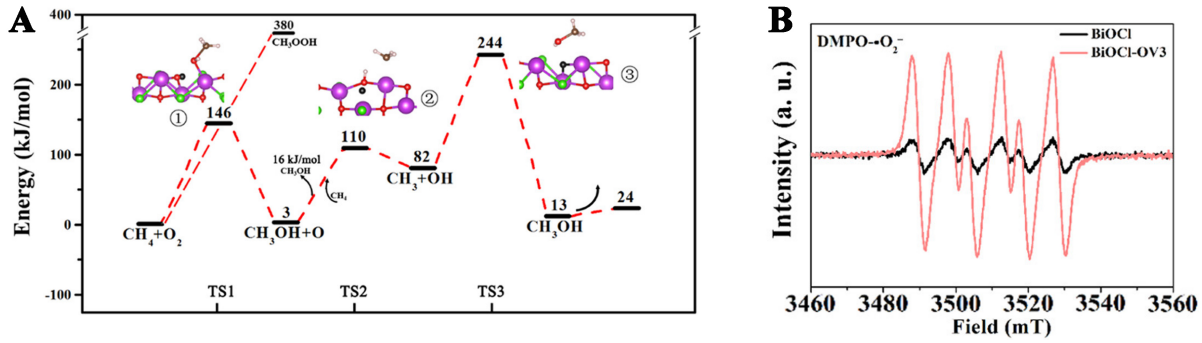

Figure 6. (A) Energy profiles of methane oxidation to methanol on the oxygen-defective BiOCl (010) surface; (B) EPR spectra of the catalyst suspension with DMPO as the spin probe. Reproduced with permission from Ref[44]. Copyright 2021, American Chemical Society. EPR: Electron paramagnetic resonance; DMPO: 5,5-dimethyl-1-pyrroline N-oxide.

radicals [Equation (3)]. As a result, the reaction becomes much more complex, leading to the formation of numerous by-products. However, the pathway for methanol production almost follows the mechanism outlined below[46,47]. Due to the presence of water, hydroxyl radicals take precedence over superoxide anion radicals in activating methane by oxidative dehydrogenation to produce methyl radicals [Equation (7)]. These methyl radicals then combine with superoxide anion radicals formed by the reaction between oxygen and conduction band electrons [Equation (21)], leading to the formation of CH_3OO^- through

$$\cdot CH_3 + \cdot O_2^- \rightarrow CH_3OO^- \tag{25}$$

This species then captures a proton to form CH_3OOH based on

$$CH_3OO^- + H^+ \rightarrow CH_3OOH \tag{26}$$

which, upon cleavage, produces a methoxy radical that subsequently reacts with water to yield methanol, as given in

$$CH_3OOH \rightarrow \cdot OCH_3 + \cdot OH \tag{27}$$

$$\cdot OCH_3 + H_2O \rightarrow CH_3OH + \cdot OH \tag{28}$$

The pathway of partial oxidation of methane in the presence of water almost follows the universal mechanization. A typical example is a study using HSiMo/TiO_2 as a catalyst and with H_2O participation following the mechanism in 2021[46].

Coupling of methane

In the photocatalytic conversion of methane, coupling reactions are a crucial pathway that can be classified into oxidative and non-oxidative coupling based on the presence and absence of oxygen. Oxidative coupling involves oxidants, leading to the formation of oxidation products, along with by-products such as carbon dioxide and water. This process typically occurs under moderate temperatures and requires photocatalysts with high oxygen activation ability. However, the challenge lies in controlling the reaction to avoid over-oxidation, which can reduce selectivity towards the desired products. Non-oxidative coupling occurs in the absence of oxygen, where methane molecules couple directly to form products such as ethane with minimal by-products. This reaction generally requires higher temperatures and often involves catalysts that promote

C–C bond formation. Non-oxidative coupling is advantageous for its higher selectivity, but the harsh conditions required can limit its practical application. Recent research in this area focuses on pathways or photocatalysts that can efficiently mediate these coupling reactions under mild conditions, with enhanced selectivity and reduced by-product formation[48-50]. Despite significant progress, challenges remain in achieving high conversion rates and selectivity simultaneously, particularly for non-oxidative coupling. This section will summarize the common reaction mechanisms for both types of coupling processes.

Oxidative coupling of methane

Oxidative coupling reactions mainly mediated by •OH

The hydroxyl radical-mediated oxidative coupling reactions can be broadly categorized into two main types: using only water as the reactant[51-53] and employing both water and carbon dioxide. In the water-only reaction, hydroxyl radicals are generated as previously given [Equation (3)], which oxidize methane by dehydrogenation to produce methyl radicals. These methyl radicals then follow one of two pathways to form either multi-carbon alkanes or polyols. In the first pathway, two methyl radicals couple to form ethane based on

$$2 \cdot CH_3 \rightarrow CH_3CH_3 \tag{29}$$

In the second pathway, the methyl radical combines with a hydroxyl radical to form methanol [Equation (8)]. Methanol is subsequently oxidized to generate a hydroxymethyl radical, as given in

$$CH_3OH + \cdot OH \rightarrow \cdot CH_2OH \tag{30}$$

which then couples to form ethylene glycol through

$$2 \cdot CH_2OH \rightarrow HOCH_2CH_2OH \tag{31}$$

A study published in 2021[51] used WO_3 as the catalyst adhered to this mechanism [Figure 7A]. The EPR spectrum in this study, showing the peak corresponding to the hydroxymethyl radical, confirms the reaction mechanism [Figure 7B]. When an external voltage (1.1 V *vs.* SHE) was applied, the selectivity for ethylene glycol achieved 60% in this work [Figure 7C].

Due to the involvement of multiple-step oxidation reactions and coupling processes, this reaction generally exhibits lower selectivity compared to partial oxidation reactions. Consequently, extensive research has focused on coupling electrocatalysis to optimize oxidative coupling for ethylene glycol production.

Besides the coupling of methane, another reaction pathway to form C–C bonds, hence producing C2 from C1, involves carbon dioxide and water as reactants. In such a pathway, methane still reacts with hydroxyl radicals generated from water to form methyl radicals. The critical difference is the involvement of carbon dioxide. Carbon dioxide captures photogenerated electrons to form an anion through

$$CO_2 + e^- \rightarrow \cdot CO_2^- \tag{32}$$

which then couples with protons and the previously formed methyl radicals to produce acetic acid, as given in

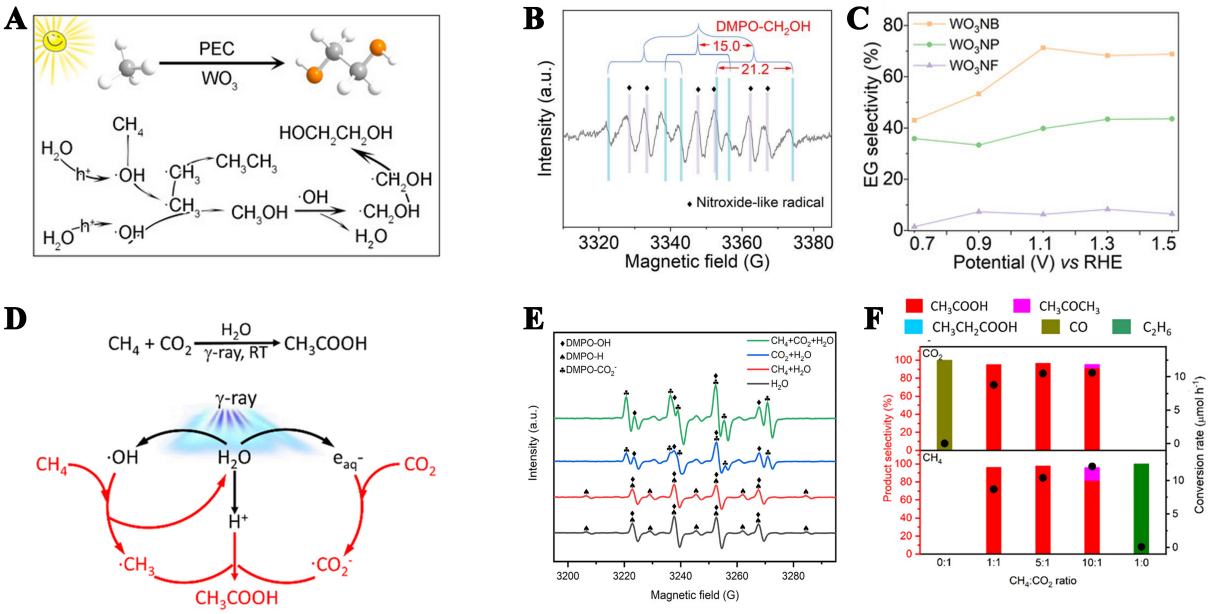

Figure 7. (A) Schematic illustration of the proposed reaction mechanism for CH_4 conversion into ethylene glycol; (B) EPR spectra of the catalyst suspension with DMPO as the spin probe; (C) The selectivity of CH_4 conversion into ethylene glycol. Reproduced with permission from Ref[51]. Copyright 2021, Wiley-VCH; (D) Schematic illustration of water radiocatalysis for aqueous-phase CH_4 carboxylation with CO_2 to CH_3COOH at RT under γ-ray radiation; (E) EPR spectra of 0.1 MPa Ar 100 mL H_2O + 150 μL DMPO (black), 0.1 MPa CH_4 + 100 mL H_2O + 150 μL DMPO (red), 0.1 MPa CO_2 + 100 mL H_2O + 150 μL DMPO (blue) and 0.1 MPa CH_4 and CO_2 mixture (CH_4:CO_2 = 5:1) + 100 mL H_2O + 150 μL DMPO (green) after γ-ray irradiation for 2 h at 298 K; (F) Conversion rates of CH_4 and CO_2 and product selectivity calculated from CH_4 and CO_2 radiated for 6 h at RT under 0.1 MPa 40 mL of CH_4 and CO_2 mixtures with different CH_4:CO_2 ratios and 100 mL of H_2O. Reproduced with permission from Ref[54]. Copyright 2024, American Chemical Society. EPR: Electron paramagnetic resonance; DMPO: 5,5-dimethyl-1-pyrroline N-oxide; RT: room temperature.

$$\cdot CH_3 + CO_2^- + H^+ \rightarrow CH_3COOH \quad (33)$$

As shown in Figure 7D, methane oxidation could be achieved in the presence of carbon dioxide and water, followed by coupling to produce acetic acid, following the reaction mechanism outlined above[54]. The EPR spectrum confirmed the presence of crucial radical species, including hydroxyl radicals and $\cdot CO_2^-$ [Figure 7E]. When the ratio of methane to carbon dioxide was optimized, the selectivity for acetic acid reached nearly 100% [Figure 7F].

It should be noted that the hydroxyl radicals can be in the presence of both the partial oxidation and the oxidative coupling of methane, as mentioned above in Section 2.1.1. In both reactions, methane can be oxidized to $\cdot CH_3$ and $\cdot CH_2OH$ radicals. The key difference is that in the oxidative coupling reaction, $\cdot CH_3$ radicals react with another $\cdot CH_3$ radical to form hydrocarbon, while the $\cdot CH_2OH$ radicals react with another $\cdot CH_2OH$ to form polyols. Both intermediates are not preferred to be further oxidized by hydroxyl radicals. To some extent, partial oxidation and oxidative coupling involve similar steps and are competitive. Such selectivity is highly dependent on the tailoring of reaction sites for coupling, the concentration of hydroxyl radicals, the contact mode with the substrate, the selective adsorption of the active site of the catalyst, and so on.

Oxidative coupling reactions mainly mediated by $\cdot O_2^-$

Different from ·OH, when $\cdot O_2^-$ participates in the reaction, the product is usually hydrocarbon. This is because $\cdot O_2^-$ just promotes the production of $\cdot CH_3$, and the common photocatalysts are mainly ZnO and

TiO_2, which influences the mechanism. This section discusses the mechanisms of methane oxidative coupling reactions involving $\bullet O_2^-$ based on these two types of photocatalysts.

Firstly, in the case of oxidative coupling reactions using TiO_2 as the photocatalyst, the thermodynamic oxidation potential of the holes in the valence band of TiO_2 is more positive than the potential required for methane dehydrogenation. This allows TiO_2 to dehydrogenate methane, forming methyl radicals directly. Consequently, the primary role of oxygen is to combine with photogenerated electrons to form superoxide anion radicals, which promote the separation of electron-hole pairs and enhance the efficiency of methane oxidation by holes[55,56]. In this type of reaction, methane is typically directly oxidized by the photocatalyst, leading to the coupling of methyl radicals at active sites to form multi-carbon alkanes, following the mechanisms given in

$$Ti^{4+}O_2^{2-} + h\nu \rightarrow Ti^{3+}O^-O^{2-} \tag{34}$$

$$O_2 + e^- \rightarrow \cdot O_2^- \tag{35}$$

$$CH_4 + h^+ \rightarrow \cdot CH_3 + H^+ \tag{36}$$

$$2 \cdot CH_3 \rightarrow C_2H_6 \tag{37}$$

$$C_2H_6 + h^+ \rightarrow \cdot C_2H_5 + H^+ \tag{38}$$

$$\cdot C_2H_5 + \cdot CH_3 \rightarrow C_3H_8 \tag{39}$$

The key to improving the selectivity for ethane and other multi-carbon alkanes in these reactions lies in inhibiting the further oxidation of methyl radicals by superoxide anion radicals or preventing excessive oxidation of methyl radicals by holes.

A common method to inhibit further oxidation by superoxide anion radicals is to convert them into stable, neutral species. To prevent excessive oxidation of methyl radicals by holes, constructing heterojunctions is often used to modify the thermodynamic oxidation potential of the system. As shown in Figure 8A, a TiO_2 photocatalyst decorated with an Ag/AgBr heterostructure[56], where electrons are extracted by Ag from the conduction band of TiO_2 then rapidly consumed by oxygen, hence facilitating efficient electron-hole separation. The holes in the valence band of TiO_2 are transferred to the VB of AgBr, leading to a milder methane oxidation process by the less oxidative holes in the VB of AgBr. As a result, this system achieved an ethane selectivity of 80% with a yield of 40 μmol/h and stability for up to 12 h [Figure 8B]. Another approach [Figure 8C] converts oxygen into more stable water, which not only consumes conduction band electrons to promote carrier separation but also utilizes Au active sites to extract holes for methane dehydrogenation and coupling, achieving a C_2 product yield of approximately 450 μmol/h with sustained stability for 30 h [Figure 8D][55].

Another commonly used photocatalyst is ZnO, which exhibits unique properties that influence the reaction mechanism, as given in[57,58]

$$Zn^{2+}O^{2-} + h\nu \rightarrow Zn^+O^- \tag{40}$$

$$O_2 + H_2O \rightarrow \cdot O_2 + \cdot OH + \cdot H \tag{41}$$

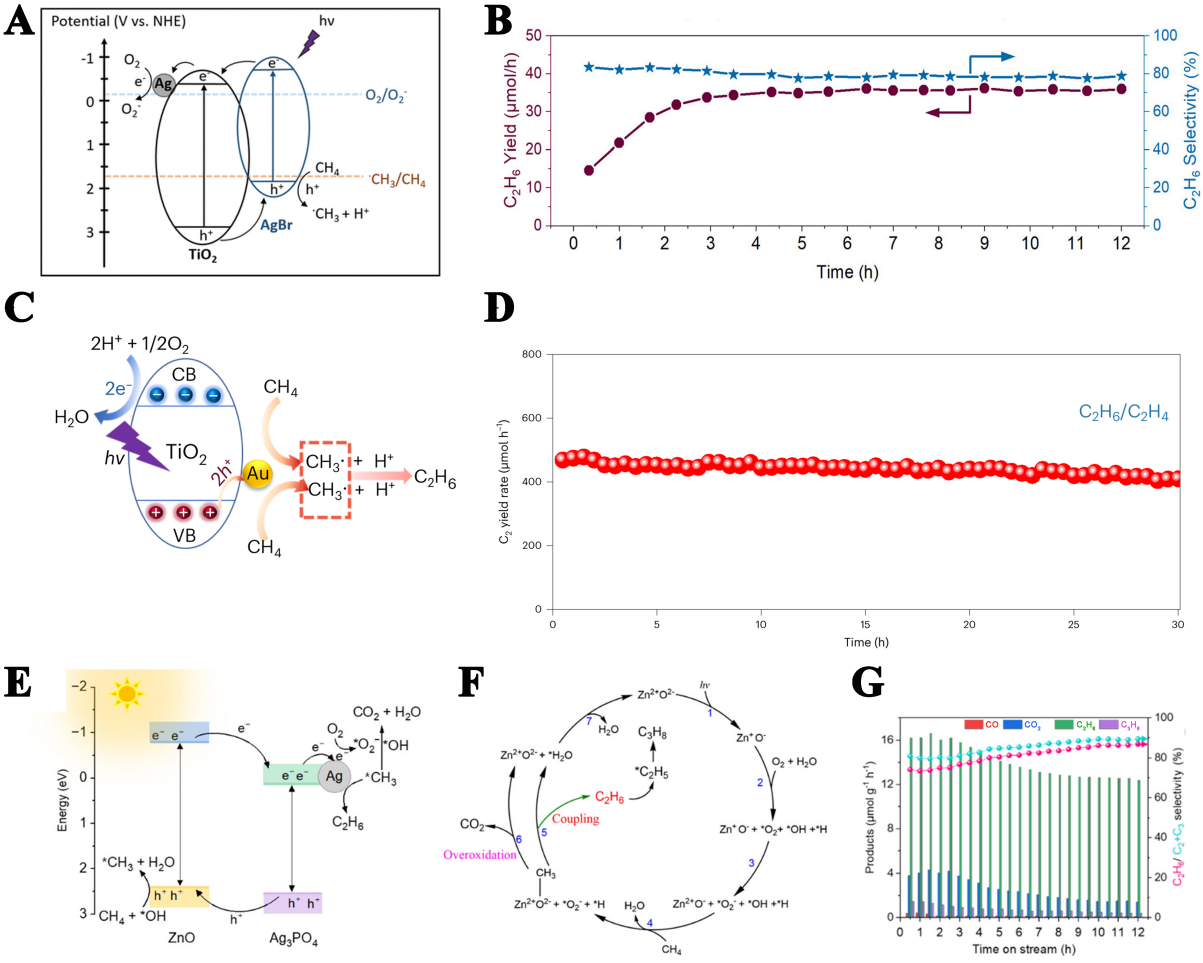

Figure 8. (A) Photocatalytic Reaction Pathway of Ag–AgBr/TiO_2; (B) Long-term C_2H_6 production rate and selectivity under 6 bar pressure over Ag–AgBr/TiO_2. Reproduced with permission from Ref[56]. Copyright 2023, American Chemical Society; (C) Proposed photocatalytic oxidative coupling of methane process over Au/TiO_2; (D) Stability test of Au/TiO_2 under the optimized reaction condition (reaction condition: 20 mg TiO_2, 320 mL/min CH_4, 12 mL/min air, 393 K, 365 nm LED 100 W). Reproduced with permission from Ref[55]. Copyright 2023, Springer Nature; (E) Schematic illustration of the proposed reaction mechanism for photocatalytic OCM to C_2H_6 using O_2 and H_2O on Ag_3PO_4-ZnO from the energy band structure and (F) the reaction mechanism; (G) Continuous stability tests in photocatalytic oxidative coupling of methane process on Ag_3PO_4-ZnO. Reproduced with permission from Ref[58]. Copyright 2023, American Chemical Society. LED: Light emitting diode; OCM: oxidative coupling of methane.

$$\cdot O_2 + Zn^+O^- \rightarrow \cdot O_2^- + Zn^{2+}O^- \tag{42}$$

$$CH_4 + Zn^+O^- + \cdot OH \rightarrow Zn^{2+}O^{2-} + H_2O + \cdot CH_3 \tag{43}$$

$$2 \cdot CH_3 \rightarrow C_2H_6 \tag{44}$$

In the case of ZnO modified with Ag_3PO_4 as the catalyst, by leveraging the appropriate bandgap structures of ZnO and Ag_3PO_4, a heterojunction between ZnO and Ag_3PO_4 was successfully formed [Figure 8E][58]. The electrons on ZnO are transferred to Ag_3PO_4 at first under illumination to form Ag nanoparticles [Equation (40)].

Photogenerated electrons transfer to Ag NPs and are consumed by O_2 to form superoxide anion radicals accompanied by H_2O dissociation to form hydroxyl radicals on ZnO [Equations (41 and 42)].

Subsequently, the hydroxyl radicals oxidize methane to form methyl radicals, which then couple to form ethane [Equations (43 and 44)] [Figure 8F].

Due to the presence of O_2 and H_2O, in particular, speeding up the separation and utilization of photogenerated electrons and holes, the selectivity of C2 and C2+ reaches 80%, and the stability of the system holds for 12 h [Figure 8G].

It should be noted that oxidants can not only react with photoelectrons, leaving holes to oxidize methane, but they can also directly react with methane. For example, oxygen can react with methane on the ZnO photocatalyst, leading to the production of carbon dioxide[15].

Non-oxidative coupling of methane

The photocatalytic non-oxidative coupling of methane is a process in which methane molecules are activated and directly coupled to form higher hydrocarbons, such as ethane, without the involvement of oxygen[48,59,60]. This method is often used in systems where the presence of oxygen could lead to undesirable over-oxidation and consequently reduce the selectivity towards the desired C–C coupling products[61,62]. One of the main advantages of non-oxidative coupling is its ability to produce valuable hydrocarbons while minimizing the formation of by-products such as carbon dioxide[63,64]. However, this approach faces significant challenges, including the high activation energy required to break the strong C–H bonds in methane due to the absence of oxidant and the tendency for side reactions that can lead to coke formation or the production of unwanted by-products. Moreover, identifying suitable catalysts that offer both high selectivity and stability under reaction conditions remains a significant obstacle in this technology.

The non-oxidative coupling process involves the holes in the valence band of a photocatalyst instead of any oxidant to directly oxidize and dehydrogenate methane, followed by coupling[61-66]

$$CH_4 + h^+ \rightarrow \cdot CH_3 + H^+ \quad (45)$$

$$2 \cdot CH_3 \rightarrow C_2H_6 \quad (46)$$

$$C_2H_6 + h^+ \rightarrow \cdot C_2H_5 + H^+ \quad (47)$$

$$\cdot C_2H_5 + \cdot CH_3 \rightarrow C_3H_8 \quad (48)$$

$$2 \cdot C_2H_5 \rightarrow C_4H_{10} \quad (49)$$

In this process, many studies focus on the catalyst which can achieve the production of C_2H_6 with high selectivity. However, the production rate is much lower compared with the oxidative coupling process. This is because the activation of methane is limited in the absence of oxidant. Therefore, the challenge for non-oxidative coupling lies in enhancing the production rate of C2 products under mild conditions. Regarding selectivity, the focus should be more on C3 products. And the production of hydrocarbons larger than C_4H_{10} is nearly impossible to occur, probably due to the challenging absorption of C_3H_8. The following section introduces the development of some widely used catalysts.

In 2019, a Mott–Schottky photocatalyst was fabricated by loading Pt nanoclusters on a Ga-doped hierarchical porous TiO_2–SiO_2 microarray with an anatase framework, which exhibits a CH_4 conversion rate of 3.48 μmol·g^{-1}·h^{-1} with 90% selectivity toward C_2H_6 [Figure 9A][59]. Besides, an n-type photocatalyst synthesized via doping single-atom Nb into hierarchical porous TiO_2–SiO_2 microarray exhibits a high conversion rate of 3.57 μmol/g/h with good recyclability [Figure 9B][60]. In 2022, a catalyst Pd-modified TiO_2

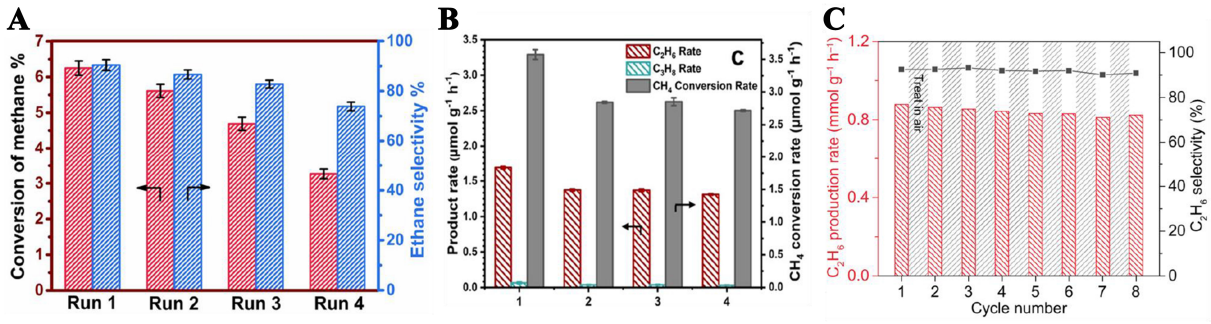

Figure 9. (A) Cycle photo-driven methane non-oxidative coupling reaction over Ga-doped hierarchical porous Pt-TiO_2–SiO_2(2%). Every run is carried out under direct irradiation from a 300 W Xe lamp for 4 h. Reproduced with permission from Ref[59]. Copyright 2019, American Chemical Society; (B) The cycle of photocatalytic methane non-oxidative coupling reactions over TiO_2–SiO_2. Reproduced with permission from Ref[60]. Copyright 2021, Wiley-VCH; (C) Production rates and selectivity of C_2H_6 in the cyclic tests by Pd/TiO_2. Each cycle lasts 3 h, during which the catalyst is treated in air. Reproduced with permission from Ref[48]. Copyright 2023, Springer Nature.

exhibits good performance toward C_2H_6 production, with an apparent quantum efficiency of 3.05% at 350 nm and an extraordinary C_2H_6 production rate of 0.91 mmol·g^{-1}·h^{-1}. More importantly, the occupied state of Pd–O in the VB maximum suppresses the overoxidation of CH_4 with lattice oxygen, which achieves 94.3% selectivity toward C_2H_6 production and substantially improved stability of oxide photocatalyst [Figure 9C][48].

Functionalization of methane

In recent years, photocatalytic functionalization of methane has emerged as a versatile approach, enabling a range of chemical transformations such as boronation, nitration, and halogenation. Boronation of methane typically involves the use of photocatalysts to introduce boron atoms into the methane molecule and yields products such as methylboranes, which are valuable in the synthesis of organoboron compounds. Nitration of methane, on the other hand, involves the incorporation of nitro groups, resulting in products such as methyl nitrates. Such compounds are used in the production of pharmaceuticals and explosives. However, the nitration of methane faces challenges such as low selectivity and the need for controlled reaction conditions to avoid the formation of undesired by-products. Halogenation of methane introduces halogen atoms (such as chlorine or bromine) into the molecule. It produces methyl halides, which are essential in various industrial applications, including the manufacture of agrochemicals and pharmaceuticals. The primary challenges in the halogenation of methane include managing the reaction's selectivity and avoiding excessive halogenation, which can lead to complex mixtures of products. Overall, while photocatalytic methods for methane functionalization hold significant promise, they are often hindered by issues such as reaction efficiency, selectivity, and the need for optimization of reaction conditions. It is crucial to address these challenges for advancing these processes in practical applications.

Halogenation of methane

Photocatalytic halogenation of methane is a reaction frequently employed in organic chemistry, particularly for the synthesis of halogenated hydrocarbons. In this reaction, methane is exposed to light in the presence of a halogen, such as chlorine or bromine, leading to the formation of a methyl radical and a halogen radical, as given in

$$CH_4 + h^+ \rightarrow \cdot CH_3 + H^+ \quad (50)$$

$$Cl^- + h^+ \rightarrow \cdot Cl \quad (51)$$

The radicals subsequently react to produce halogenated methane, such as chloromethane or bromomethane, as the primary product, as given in[67,68]

$$\cdot CH_3 + \cdot Cl \rightarrow CH_3Cl \quad (52)$$

However, the reaction often results in over-halogenation, leading to the formation of by-products such as dichloromethane, chloroform, or even carbon tetrachloride when chlorine is used. The selectivity of the reaction can be a significant challenge, as controlling the extent of halogenation is difficult, limiting the efficiency of the process and complicating the purification of the desired product. The primary research direction in methane photocatalytic halogenation is the development of a system that can enhance the selectivity and yield of the desired products while minimizing by-products. For example, Cu-doped TiO_2 affords a methyl halide production rate of up to 0.61 mmol/h/m^2 for chloromethane [Figure 10A], accompanied by a selectivity > 80% [Figure 10B] due to Cu stabilizing the methyl radicals for its coupling with Cl^- to form the targeted CH_3Cl, which are further proven transformable to methanol and pharmaceutical intermediates[68]. It can also operate solely in the presence of seawater and methane, showing its potential for practical offshore methane exploitation.

Alongside stabilizing the intermediate methyl radical species, another strategy to enhance selectivity and yield for halomethane involves mitigating the peroxidation of methyl radicals. Li *et al.* reported that loading silver oxide nanoparticles into the catalyst significantly reduces the concentration of hydroxyl radicals, thereby stabilizing the methyl radicals [Figure 10C and D][67]. This enhancement in methyl radical selectivity culminated in an impressive CH_3Cl yield of 152 μmol·g^{-1}·h^{-1}.

In summary, as a crucial component of photocatalytic methane functionalization, halogenation represents a critical direction with a relatively unified reaction mechanism - primarily involving the coupling reaction between methyl radicals and chlorine radicals, and the key lies in constructing active sites for coupling reactions and stabilizing methyl radical while suppressing the excessive oxidation of carbon-hydrogen bonds for improve selectivity.

Nitration of methane

Photocatalytic methane nitration is a process that typically involves the activation of methane using light in the presence of a photocatalyst to facilitate the introduction of a nitro group (-NO_2) into the methane molecule. This reaction is often conducted under UV light, the reactive species that interact with methane and a nitrogen source, typically nitric acid or nitrogen dioxide, to produce nitromethane as the desired product. In this process, despite the oxidants commonly used in traditional methane oxidation or coupling processes (i.e., H_2O, H_2O_2), the nitration process itself is challenging in terms of directly introducing nitrogen into the methane molecule. A halogen radical with higher selectivity is commonly required as an activator to selectively generate methyl radical intermediates [Figure 11]. For instance, He *et al.* used $AlCl_3$/$Al(NO_3)_3$ as the nitration source and catalyst[69], obtaining a methane conversion of 17% and CH_3ONO_2 selectivity of 78% at 100 °C through

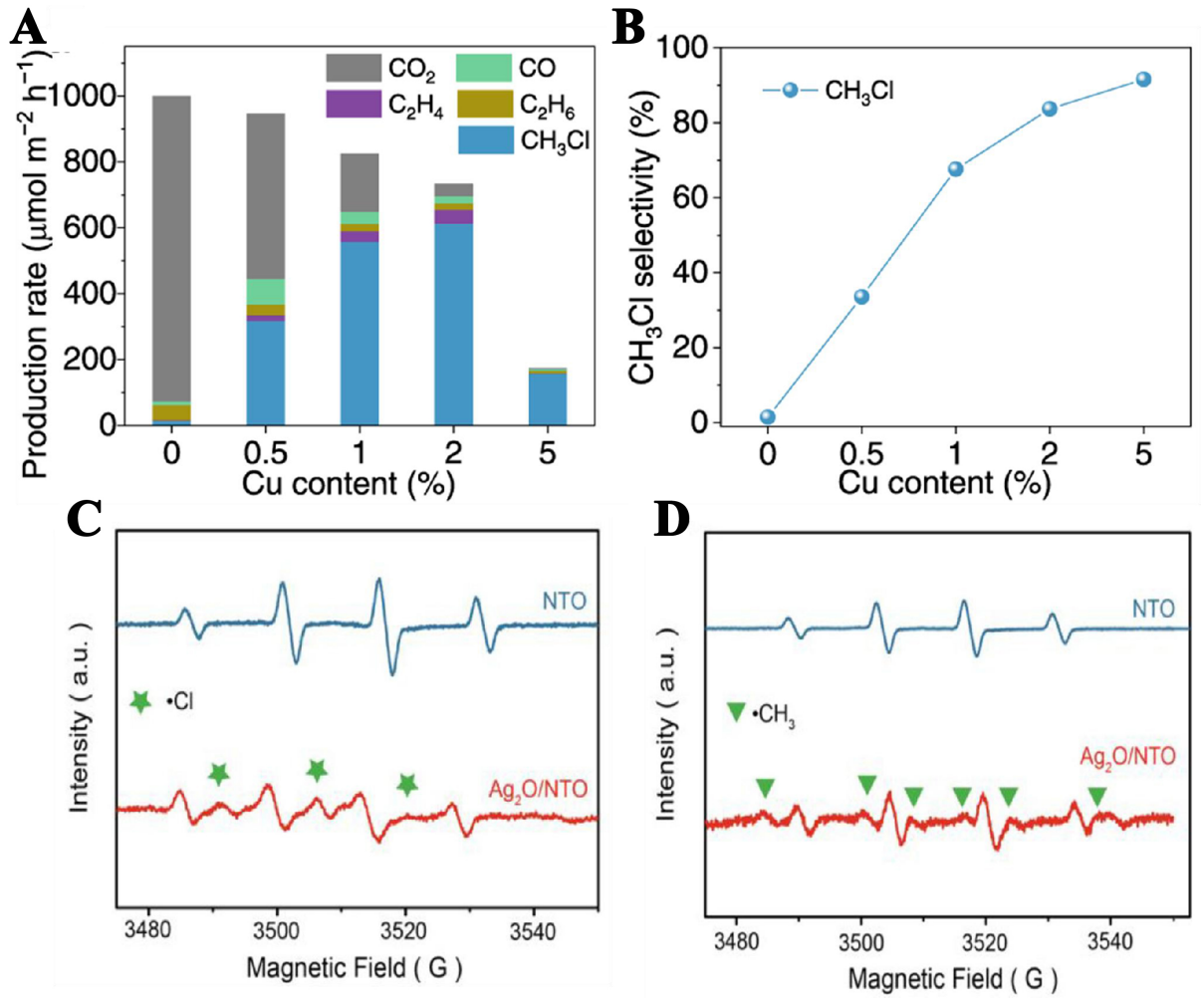

Figure 10. Photocatalytic methane halogenation efficiency (A) and selectivity (B) of *X*% Cu–TiO_2 toward CH_3Cl production. Reproduced with permission from Ref[68]. Copyright 2023, Springer Nature. Radical signal of EPR spectra of (C) Cl radical and (D) methyl radical over NTO and 0.5 wt% Ag_2O/NTO. Reproduced with permission from Ref[67]. Copyright 2022, American Chemical Society. EPR: Electron paramagnetic resonance.

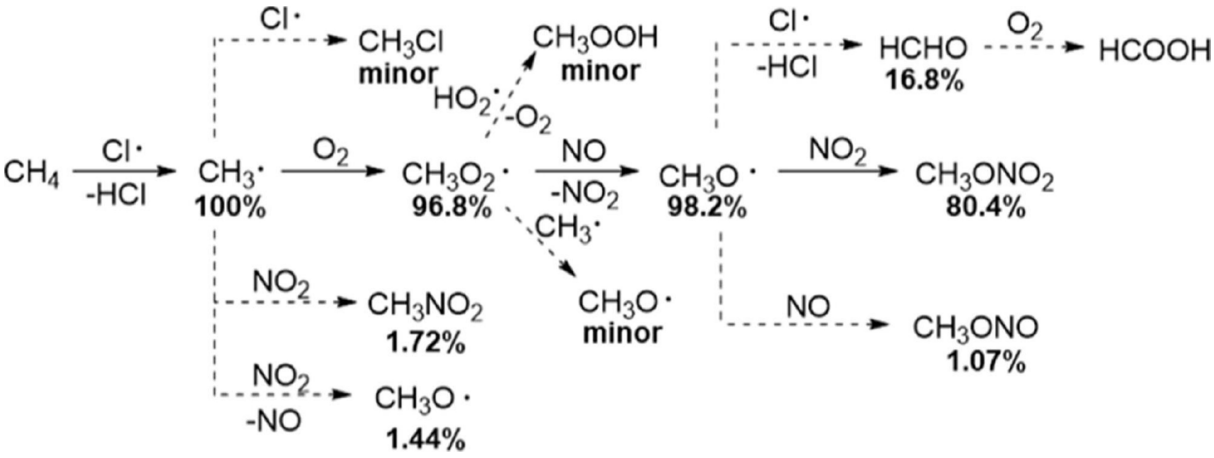

Figure 11. Sketch diagram of the conversion pathway from methane to methyl nitrate. The dotted arrows refer to side reactions, and the solid arrows refer to the primary process. Reproduced with permission from Ref[69]. Copyright 2024, American Chemical Society.

$$CH_4 + \cdot Cl \rightarrow \cdot CH_3 + HCl \quad (53)$$

$$\cdot CH_3 + O_2 \rightarrow \cdot CH_3O_2 \quad (54)$$

$$\cdot CH_3O_2 + NO \rightarrow NO_2 + \cdot OCH_3 \quad (55)$$

$$\cdot OCH_3 + NO_2 \rightarrow CH_3ONO_2 \quad (56)$$

In summary, as a component of photocatalytic methane functionalization, methane nitration still has much to explore, as only a few researchers are involved.

Borylation of methane

Photocatalytic methane borylation is a promising method for directly functionalizing methane by introducing a boron group under light irradiation. Typically, this process employs a photocatalyst, such as a transition metal complex or a semiconductor, along with a borylating reagent, including bis(pinacolato) diboron (B_2pin_2)[70]. Traditionally, this reaction relies on noble metal catalysts for C–H bond cleavage[71] [Figure 12]. In contrast, photocatalytic processes often employ a hydrogen atom transfer, and the C–H bond is cleaved by intermolecular reaction with a heteroatom-centered radical under irradiation and subsequently forms the C–B bond by reaction between the resulting methyl radical intermediate and a diboron reagent. Compared to activation strategies in other methane conversion methods, this approach involves a non-activated, radical-initiated process utilizing a radical-mediated hydrogen atom transfer mechanism[73].

Reforming of methane

Dry reforming and steam reforming of methane are two key processes used to convert methane into valuable products. Due to the high temperatures required to activate reactants in the reforming process, most current research employs a combination of light and thermal energy for methane reforming. Consequently, achieving methane reforming at lower temperatures using photocatalysis remains a significant challenge[74-76]. First, dry reforming involves the reaction of methane with carbon dioxide to produce syngas, which is a mixture of hydrogen and carbon monoxide[77-79]. Dry reforming uses carbon dioxide as a reactant, which can help mitigate the emission of greenhouse gases and contribute to carbon capture and storage. However, dry reforming typically requires a high temperature to achieve adequate reaction rates, which can increase energy consumption and operational costs. Besides, the process can lead to the formation of carbon deposits on the catalyst, which causes the deactivation of reactive sites and reduces the efficiency of the process over time. Therefore, the stability and deactivation resistance of the catalyst is essential. The mechanism of the process is given as follows

$$CO_2 + 2e^- \rightarrow O^{2-} + CO \quad (57)$$

$$CH_4 + 2h^+ + O^{2-} \rightarrow 2H_2 + CO \quad (58)$$

which has been reported in many versions in detail though using the same catalyst, so we introduce a brief but accurate version[78-81].

As reported in 2020, a plasmonic photocatalyst consisting of a Cu nanoparticle antenna with single-Ru atomic reactor sites on the nanoparticle surface [Figure 13A] is ideal for low-temperature, light-driven methane dry reforming[74]. This catalyst provides high efficiency of light energy utilization when illuminated at room temperature. In contrast to thermal catalysis, long-term stability (50 h) and very high selectivity (> 99%) were achieved in photocatalysis [Figure 13B and C][74]. In 2022, a surface-modulation strategy is demonstrated via decorating *in situ* defects on isolated nickel (Ni) atoms over La_2O_3 for boosting light-driven dry reforming of methane activity [Figure 13D]. Atomically dispersed Ni/La_2O_3 achieves a hydrogen evolution rate of 70.9 mol·g_{Ni}^{-1}·h^{-1} [Figure 13E][79].

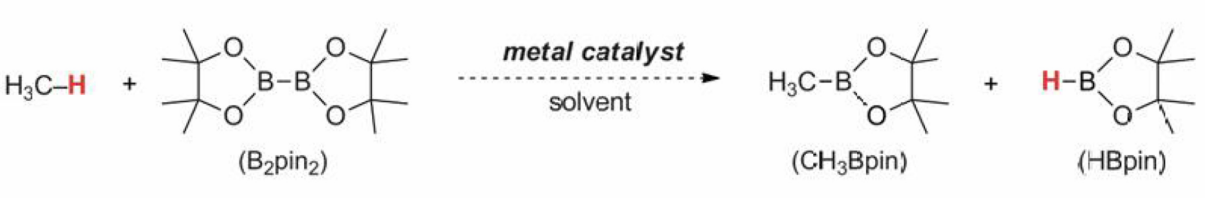

Figure 12. Reactivity and selectivity in the C–H borylation of methane Reproduced with permission from Ref[72]. Copyright 2016, American Association for the Advancement of Science.

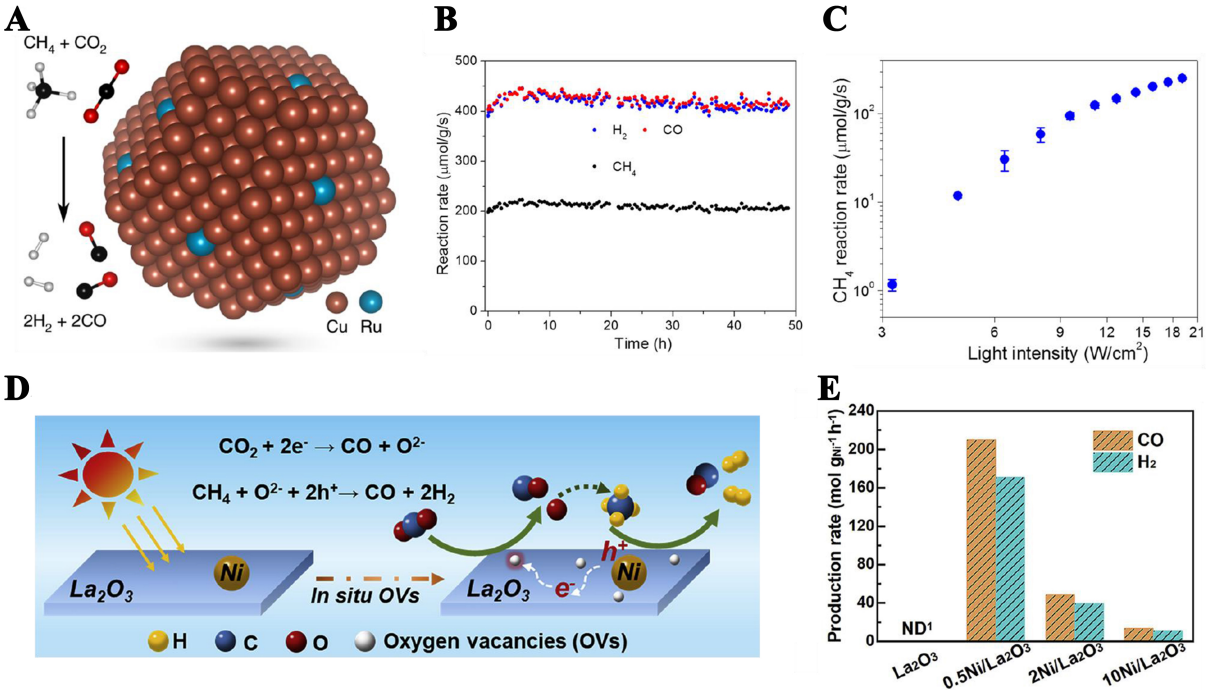

Figure 13. (A) Schematic of a Cu–single-atom Ru surface alloy catalyst with the dry reforming reactants and products shown on the left; (B) Stability of photocatalytic methane dry reforming reaction on a Cu-Ru catalyst under 19.2 W·cm^{-2} white light illumination. The flow rates of CH_4 and CO_2 were both 8 sccm; (C) Intensity dependence of photocatalytic methane dry reforming reaction on Cu-Ru catalyst. No external heating was applied. Reproduced with permission from Ref[74]. Copyright 2020, Springer Nature; (D) Schematic of the dynamics within light-driven photothermal methane dry reforming; (E) Production rates of H_2 and CO in 3 h. Reaction conditions: 10 mg samples were under focused full-spectrum light irradiation (21.6 W/cm^2) with a continuous flow of 8 vol% CO_2, 8 vol% CH_4, and 84 vol% Ar with a rate of 90 mL/min. Reproduced with permission from Ref[79]. Copyright 2022, Elsevier.

Another photocatalytic methane reforming technique involves the presence of water to produce syngas, known as steam reforming. Steam reforming produces less carbon accompanied by large quantities of hydrogen compared to dry reforming, leading to fewer issues with catalyst deactivation from carbon deposition. However, a primary challenge in steam reforming is to enhance methane conversion at low temperatures and ambient conditions. Currently, the conversion efficiency and syngas production rate of conventional photocatalytic methane reforming are significantly lower than those achieved through thermal catalysis at high temperatures. The reaction mechanism for photocatalytic methane steam reforming follows the steps: methane is first oxidized in the presence of water, either directly by valence band holes[7] or by hydroxyl radicals generated from water oxidation via holes[82], which is similar to the partial oxidation of methane in the presence of water. This process produces protons and carbon oxides (including CO or CO_2), while conduction band electrons subsequently reduce the protons to produce hydrogen. A typical example is the use of Rh and RhO-modified potassium titanate as a photocatalyst for methane steam reforming

[Figure 14A][7]. In this system, the hydrogen production rate can exceed 1.2 μmol/min and maintain stability for ten hours [Figure 14B]. However, a notable drawback is the inevitable production of carbon dioxide during the reaction.

The above discusses the reaction pathways of photocatalytic methane conversion. Representative work for the four aspects of photocatalytic methane conversion is summarized in Table 1.

THE MATERIALS OF PHOTOCATALYTIC METHANE CONVERSION

Similar to other photocatalytic processes, the photocatalysts commonly used for methane conversion mainly consist of semiconductor materials and metal nanomaterials. Semiconductors are primarily responsible for light absorption and photogenerated carrier generation, while metal nanomaterials are mostly used as co-catalysts to enhance the photocatalytic conversion process[3].

As mentioned above, the photocatalyst can directly activate methane only when the thermodynamic potential of the semiconductor material reaches the level required for methane activation. Commonly used photocatalysts are mainly metal oxides, nitrides, and other semiconductor materials. TiO_2 is a widely used photocatalyst and was first used for the complete oxidation of methane[83]. However, TiO_2 needs to be designed appropriately to complex different reaction systems to contribute to the enhancement of methane conversion performance, such as loading metal and metal oxide cobalt oxide (CoO_x) nanoclusters on the TiO_2 surface, which can selectively oxidize methane to methanol with selectivity up to 95%, attributed to the metal's promotion of photogenerated electron segregation and the inhibition of hydroxyl radicals by the metal oxide nanoclusters thus avoiding over-oxidation[31]. The Pd-doped TiO_2 was shown to have exceptional performance in the non-oxidative coupling of methane to ethane production, which is attributed to the doping that reduces the contribution of O 2p states to valence band near-surface, suppressing the overoxidation of CH_4 with lattice oxygen[48].

Moreover, rational regulation of the defective layer over TiO_2 is a strategy for selectively oxidizing CH_4. The optimized oxygen-vacancy-rich surface disorder layer can simultaneously promote the separation and migration of photogenerated charge carriers and enhance the activation of O_2 and CH_4 for conversion with an HCHO production rate up to 3.16 $mmol \cdot g^{-1} \cdot h^{-1}$ and 81.2% selectivity[32]. ZnO is also commonly used as a photocatalyst for methane conversion due to its inhomogeneous internal charge distribution and the existence of an intrinsic built-in electric field that facilitates methane activation[3]. For instance, the polar and nonpolar surfaces of zinc oxide have a significant effect on the methane oxidation process[8]. In addition, WO_3[84,85], Ga_2O_3[22] and other semiconductor materials with a wide bandgap are usually used in this system but with the limitations of the wide bandgap, resulting in poor visible light absorption. In addition, carbon nitride in nitrides is another class of materials for photocatalytic methane conversion. Carbon nitride has the tunability to accommodate different conversion processes. For example, Cu-modified carbon nitride can oxidize the methane to ethanol[11], while Zn-doped carbon nitride can photocatalytic coupling of methane and CO_2 into C2-hydrocarbons[86]. In addition to the commonly used oxides and nitrides, there are other ternary oxides photocatalysts, such as $SrTiO_3$ and[6,29,75] $BiVO_4$[23]. Various catalyst choices and modifications will be suitable for different reaction systems in photocatalytic methane conversion.

Aside from semiconductor materials, metallic nanoparticles can be employed to induce surface plasmon resonance, enhancing light absorption and activating methane through the localized surface plasmon resonance[16,87], which is particularly applicable to methane dry reforming reaction as the reaction requires high temperatures (700-1,100 °C)[88]. Also, introducing solar energy into the thermally driven reaction system to enhance catalyst activity, thus allowing the reaction to proceed at lower temperatures, makes it

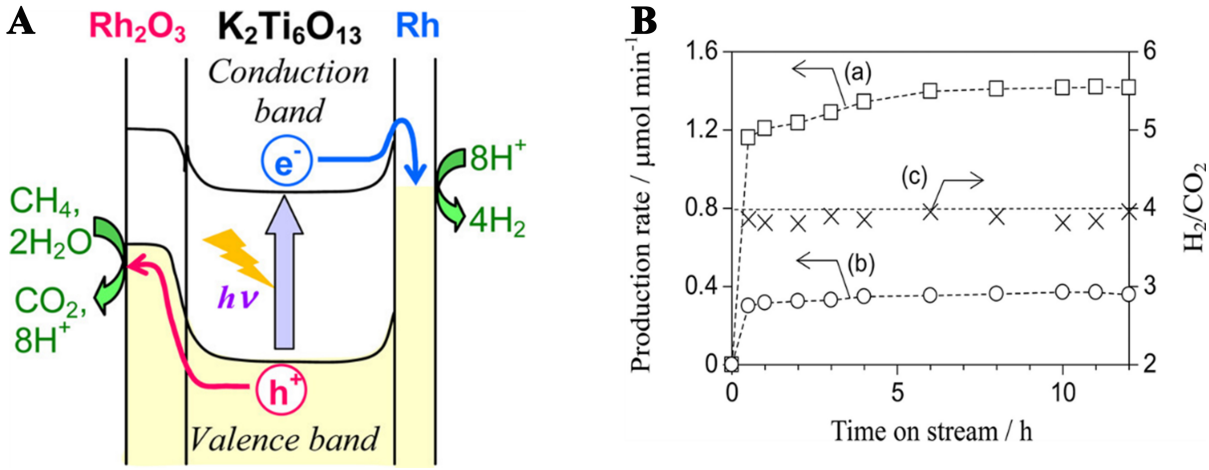

Figure 14. (A) Schematic of photocatalytic steam reforming of methane over alkaline titanate; (B) Time course of the production rate of (a) H_2 and (b) CO_2 on the $Rh/K_2Ti_6O_{13}$ sample, and (c) that of molar ratio of the produced H_2 and CO_2 (H_2/CO_2) in the flowing mixture of water vapor and methane. The Rh co-catalyst was loaded using the photodeposition method. Reproduced with permission from Ref[7]. Copyright 2012, American Chemical Society.

much more attractive. Common materials primarily include nanoparticles of Au, Cu, Ag, Pt, Ni, *etc.*[87,89]. They have strong interaction with resonant photons through excitation of surface plasmon resonance, which can relax by locally heating the nanostructure[90]. In a typical example, Ru single atoms are loaded onto Cu nanoparticles to form a plasmonic photocatalyst. The small plasmonic Cu antennas provide strong light absorption and thus efficient generation of hot carriers under illumination, while single-atom Ru sites offer a high catalytic activity for dry reforming of methane with long-term stability (50 h) and high selectivity (> 99%) at room temperature[74].

In summary, the types of photocatalysts used in methane conversion reactions are similar to those in other photocatalytic processes. However, photocatalysts with a wider bandgap are commonly employed to drive methane activation thermodynamically. The specific morphology, structure, and composition of the catalyst can be altered to suit different reaction systems, which will not be further elaborated here.

CONCLUSIONS, CHALLENGES, AND PERSPECTIVES

Photocatalytic methane conversion represents a highly promising reaction, with the study of its mechanisms being crucial. This review summarizes the pathways of photocatalytic methane conversion. Specifically, we focus on four main conversion pathways: partial oxidation, oxidative/non-oxidative coupling, functionalization, and dry/steam reforming of methane. We also outline the underlying mechanisms based on the main radical species or required reactants in each process. For photocatalytic methane conversion, the key to the conversion is the activation of methane, the control of reaction pathways, and the relationship between the factors. Although several studies have reported highly selective conversion (> 90%), the yield or selectivity of a target product remains a significant challenge. So far, photocatalysis still hardly exhibits a clear advantage over thermal catalysis in terms of yield in methane conversion.

Among the four main methods for methane conversion, the greatest challenge in partial oxidation reactions lies in balancing and regulating the methane activation with its oxidation, which directly affects product yield and selectivity. In contrast, non-oxidative coupling reactions avoid concerns over oxidation selectivity under anoxic conditions. Still, the absence of an oxidant poses difficulties in methane activation, leading to poor yields of multi-carbon alkanes. For methane reforming reactions, most current studies achieving

Table 1. Recent representative works on photocatalytic methane conversion, along with their reaction systems and performance

Reaction type	Photocatalysts	Temperature	Pressure	Light source	Main product	Main product selectivity	Rate	Main by-product	Ref.
Partial oxidation	Quantum-sized bismuth vanadate	Room temperature	2 MPa	Xe lamp, 170 mW·cm^{-2}	MeOH	96.6%	330 μmol·g^{-1}·h^{-1}	CO_2	[23]
	RuO_x/ZnO/CeO_2 nanorod	Room temperature	/	Simulated solar light irradiation	MeOH	97.7%	133.54 μmol·g^{-1}·h^{-1}	CO	[24]
	FeOOH/$Li_{0.1}WO_3$ core–shell nanorods	Room temperature	2 MPa	300 W Xenon lamp	MeOH	86%	160 μmol·g^{-1}	HCHO, CH3CHO	[27]
	W single-atom	Room temperature	0.5 MPa	Xe-lamp	C1 oxide (MeOH, CH_2OHCH_2OH, CH_3OOH)	> 99%	4,956 μmol·g^{-1}	/	[28]
	Cu/CeO_2	120 °C	1.2 MPa	300 W Xe lamp (200 ≤ λ ≤ 420 nm)	MeOH	96.2%	88.9 μmol·g^{-1}·h^{-1}	CO	[30]
	Cobalt single atom on carbon nitride	25 °C	0.8 MPa	300 W Xenon lamp (300 ≤ λ ≤ 780 nm, 170 mW·cm^{-2})	MeOH	87.22%	296 μmol·g^{-1}·h^{-1}	CH_3OOH, HCHO, HCOOH, and C_2H_5OH	[25]
	Au/Co_x/TiO_2	25 ± 2 °C	2 MPa	300 W Xe lamp (450 mW·cm^{-2}, 300-500 nm)	MeOH	95%	25.4 μmol·h^{-1}	CH_3OOH, HCHO, CO_2	[31]
	TiO_2	Room temperature	2 MPa	300 W Xe lamp (50 mW·cm^{-2} with an ultraviolet pass-filter)	HCHO	81.2%	3,160 μmol·g^{-1}·h^{-1}	CH_3OOH, HCOOH, MeOH, CO_2	[32]
	AuCu–ZnO	25 °C	2 MPa	300 W Xe lamp	HCHO	Nearly 100%	11,225 μmol·g^{-1}·h^{-1} for C1 oxygenates	CO_2	[33]
	Pd-In_2O_3	Room temperature	2 MPa	LED lamp (420 nm)	CH_3OH and CH_3OOH	82.5%	100 μmol·h^{-1} of C1 oxygenates	CO_2	[34]
	Single-atom Cu and $W^{\delta+}$	25 °C	2 MPa	LED lamp source (420 nm)	HCHO	Nearly 100%	4,979.0 μmol·g^{-1} within 2 h	CO_2	[36]
	Cu@C_3N_4	50 °C	0.1 MPa	300 W Xenon lamp equipped with a 420 nm bandpass filter	Methyl oxygenates	> 98%	1,399.3 mmol·g_{Cu}^{-1}·h^{-1} of methyl oxygenates	CO_2	[39]
	001-dominated TiO_2	25 °C	2.1 MPa	300 W Xe lamp (450 mW·cm^{-2})	MeOH	80%	4,800 μmol·g^{-1}·h^{-1}	HCHO, CO, CO_2	[45]
	Silicomolybdic-acid/TiO_2	150 °C	5 MPa	300 W xenon lamp with AM 1.5G filter	Formic acid and formaldehyde	82.4% for liquid oxygenates (mainly formic acid and formaldehyde)	/	/	[46]
Coupling	/	Room temperature	0.1 MPa	γ-Ray radiation	CH_3COOH	96%	121.9 μmol·h^{-1}	CH_3COCH_3	[54]
	Au-sputtered TiO_2	> 680 °C	/	365 nm LED 100 W	C_2 products	~90%	the methane conversion rate of 1,100 μmol·h^{-1}	CO_2	[55]

	Ag/AgBr-TiO_2	40 °C	0.6 MPa	365 nm LED	C_{2+} products	79%	354 μmol·g^{-1}·h^{-1}	CO, CO_2	[56]
	Au/ZnO	81.3 °C	0.1 MPa	365 nm LED (350 mW·cm^{-2})	C_2-C_4 products	83%	683 μmol·g^{-1}·h^{-1}	CO_2	[57]
	Au-ZnO/TiO_2	140 °C	Atmospheric pressure	300-W Xe lamp, 300-500 nm, 500 mW·cm^{-2}	C_2H_6	90%	5,000 μmol·g^{-1}·h^{-1}	CO_2	[58]
	Ga-doped and Pt-loaded porous TiO_2–SiO_2	Room temperature	/	300 W Xe lamp (450 mW/cm^2)	C_2H_6	90%	3.48 μmol·g^{-1}·h^{-1}	CO_2	[59]
	Pd-TiO_2	Room temperature	/	300 W Xe lamp	C_2H_6	94.3%	910 μmol·g^{-1}·h^{-1}	CO_2	[48]
	Ag/$NaTaO_3$	Room temperature	Atmospheric pressure	Four 8 W ultraviolet lamps	C_2H_6	89%	194 μmol·g^{-1}·h^{-1}	C_3H_8, C_4H_{10}	[62]
	GaN:ZnO solid solutions	Room temperature	/	300 W Xenon lamp	C_2H_6	98 %	> 330 μmol·g^{-1}·h^{-1}	C_3H_8, C_4H_{10}	[63]
	Nb_2O_5	Room temperature	Atmospheric pressure	300 W Xe lamp with 2,000 mW/cm^2	C_2H_6	/	1,456 μmol·g^{-1}·h^{-1}	/	[64]
Functionalization	Ag_2O/La-$NaTaO_3$	Room temperature	Atmospheric pressure	Four UV lamps with the wavelength centered at 254 nm	Chloromethane	56.5%	152 μmol·g^{-1}·h^{-1}	CO_2, C_2H_6	[67]
	Cu-TiO_2	Room temperature	Ambient pressure	300 W xenon lamp (600 mW·cm^{-2})	Chloromethane, bromomethane	83.7%	610 μmol·h^{-1}·m^{-2} for chloromethane or 1,080 μmol·h^{-1}·m^{-2} for bromomethane	CO, CO_2	[68]
Reforming	Cu-Ru	Room temperature	Ambient pressure	19.2 W·cm^{-2} white light illumination	CO, H_2	> 99%	275 μmol·g^{-1}·s^{-1}	/	[74]
	Rh-$SrTiO_3$	Room temperature	Ambient pressure	150 W Hg-Xe	CO, H_2	> 50%	0.9 μmol·mg^{-1}·min^{-1}	/	[75]
	TiO_2/g-C_3N_4/Ti_3C_2	/	0.010 MPa above the atmospheric pressure	35 W Xenon lamp (420 nm, 20 mW·cm^{-2})	CO, H_2	/	45 μmol·g^{-1}·h^{-1} for H_2 or 17·μmol·g^{-1}·h^{-1} for CO	CO_2	[76]
	Pt/CeO_2	700 °C	Ambient pressure	1.2 kW concentrated solar simulator	CO, H_2	/	400 mmol·g^{-1}·h^{-1} for H_2 500 mmol·g^{-1}·h^{-1} for CO	/	[77]
	0.5Ni/La_2O_3	641 °C	/	Full-spectrum light irradiation (21.6 W·cm^{-2})	CO, H_2	/	170.9 mol·g_{Ni}^{-1}·h^{-1} for H_2 209.8 mol•g_{Ni}^{-1}·h^{-1} for CO	/	[79]
	Rh-loaded $K_2Ti_6O_{13}$	50 °C	/	Entire wavelength region from the xenon lamp	CO_2, H_2	/	0.85 μmol·min^{-1} for H_2	/	[7]

LED: Light emitting diode.

significant reforming efficiency still require high reaction temperatures. Therefore, it remains an open area of research to explore low-temperature, high-efficiency reforming of methane under photo-assisted conditions.

Currently, substantial progress has been made in understanding the mechanisms behind photocatalytic methane conversion. Many works have identified key intermediates and reaction pathways of the reaction, providing valuable insights into the reaction of methane conversion under different conditions. These advancements have facilitated the development of more efficient and selective catalysts. However, significant challenges remain, particularly in achieving precise control over reaction selectivity and efficiency. The understanding of how to manipulate the electronic and structural properties of catalysts to desired reaction pathways while suppressing side reactions is limited. To address this issue, it is crucial to employ advanced characterization techniques in this field, particularly *in situ* characterization methods. Given the mild reaction conditions typical of photocatalysis, developing additional *in situ* research techniques is especially important for mechanistic studies.

It should be acknowledged that most current research on photocatalytic methane conversion remains at the laboratory stage, and it remains challenging to transition from small-scale to processes on pilot and industrial scales. A substantial body of research focuses on advancing high-performance catalytic systems, with a critical consideration being the economic evaluation of these systems. For industrial applications, production efficiency should meet at least the following targets: (1) the photocatalyst should have a lifespan of several months; (2) the yield rates should reach the level of 1 μmol·cm^{-3}·s^{-1} or the turnover frequency of at least around 1 s^{-1}[4]. To achieve this goal, it is essential to explore the pathways of methane photocatalytic conversion, address the fundamental limitations associated with each pathway, and overcome the bottlenecks in photocatalytic conversion to enable next-generation photocatalyst design.

Furthermore, despite achieving the targets for catalysts and performance, scaling up remains a significant challenge. This assessment encompasses various factors, including the utilization of sunlight and catalysts, production scale, capital expenditures, and raw material costs[4]. The most immediate impact lies in the effect of scale-up on light utilization. The typical scale-up strategy of dimension enlargement is not practical for photochemistry owing to photon transport limitations (i.e., attenuation effect)[19,91]. At this level, it is essential not only to consider performance and economic costs but also to address additional engineering issues, such as system safety, environmental impact, and energy consumption during operation, all of which will need to be tested.

Although several critical issues need to be addressed in the future, particularly concerning yield, energy consumption, and the practical application of photocatalytic methane conversion, the direct light-driven activation of methane into high-value chemicals and fuels remains a promising technology and represents a significant scientific interest.

DECLARATIONS

Acknowledgments

Wang, Y. thanks the National Natural Science Foundation of China (52203349), the Teli Young Scholar Fellowship, and the Footecarbon Co., Ltd. for financial support.

Authors' contributions

Devised the scope and structure of the review and supervised the project: Wang, Y.

Summarized the literature accordingly: Xiong, Y.
Wrote the manuscript with contributions from all authors: Liu J.

Availability of data and materials
Not applicable.

Financial support and sponsorship
National Natural Science Foundation of China (52203349), the Teli Young Scholar Fellowship, and the Footecarbon Co., Ltd.

Conflicts of interest
All authors declared that there are no conflicts of interest.

Ethical approval and consent to participate
Not applicable.

Consent for publication
Not applicable.

REFERENCES
1. Meng, X.; Cui, X.; Rajan, N. P.; Yu, L.; Deng, D.; Bao, X. Direct methane conversion under mild condition by thermo-, electro-, or photocatalysis. *Chem* **2019**, *5*, 2296-325. DOI
2. Schwach, P.; Pan, X.; Bao, X. Direct conversion of methane to value-added chemicals over heterogeneous catalysts: challenges and prospects. *Chem. Rev.* **2017**, *117*, 8497-520. DOI PubMed
3. Bauer, N.; Hilaire, J.; Brecha, R. J.; et al. Assessing global fossil fuel availability in a scenario framework. *Energy* **2016**, *111*, 580-92. DOI
4. Li, X.; Wang, C.; Tang, J. Methane transformation by photocatalysis. *Nat. Rev. Mater.* **2022**, *7*, 617-32. DOI
5. Van Gerven, T.; Mul, G.; Moulijn, J.; Stankiewicz, A. A review of intensification of photocatalytic processes. *Chem. Eng. Process.* **2007**, *46*, 781-9. DOI
6. Pan, X.; Chen, X.; Yi, Z. Photocatalytic oxidation of methane over $SrCO_3$ decorated $SrTiO_3$ nanocatalysts *via* a synergistic effect. *Phys. Chem. Chem. Phys.* **2016**, *18*, 31400-9. DOI
7. Shimura, K.; Kawai, H.; Yoshida, T.; Yoshida, H. Bifunctional rhodium cocatalysts for photocatalytic steam reforming of methane over alkaline titanate. *ACS. Catal.* **2012**, *2*, 2126-34. DOI
8. Li, Z.; Boda, M. A.; Pan, X.; Yi, Z. Photocatalytic oxidation of small molecular hydrocarbons over ZnO nanostructures: the difference between methane and ethylene and the impact of polar and nonpolar facets. *ACS. Sustain. Chem. Eng.* **2019**, *7*, 19042-9. DOI
9. Li, Q.; Ouyang, Y.; Li, H.; Wang, L.; Zeng, J. Photocatalytic conversion of methane: recent advancements and prospects. *Angew. Chem. Int. Ed. Engl.* **2022**, *61*, e202108069. DOI
10. Murcia-López, S.; Villa, K.; Andreu, T.; Morante, J. R. Partial oxidation of methane to methanol using bismuth-based photocatalysts. *ACS. Catal.* **2014**, *4*, 3013-9. DOI
11. Zhou, Y.; Zhang, L.; Wang, W. Direct functionalization of methane into ethanol over copper modified polymeric carbon nitride via photocatalysis. *Nat. Commun.* **2019**, *10*, 506. DOI PubMed PMC
12. Xie, J.; Jin, R.; Li, A.; et al. Highly selective oxidation of methane to methanol at ambient conditions by titanium dioxide-supported iron species. *Nat. Catal.* **2018**, *1*, 889-96. DOI
13. Song, H.; Meng, X.; Wang, Z.; Liu, H.; Ye, J. Solar-energy-mediated methane conversion. *Joule* **2019**, *3*, 1606-36. DOI
14. Li, Z.; Pan, X.; Yi, Z. Photocatalytic oxidation of methane over CuO-decorated ZnO nanocatalysts. *J. Mater. Chem. A.* **2019**, *7*, 469-75. DOI
15. Chen, X.; Li, Y.; Pan, X.; Cortie, D.; Huang, X.; Yi, Z. Photocatalytic oxidation of methane over silver decorated zinc oxide nanocatalysts. *Nat. Commun.* **2016**, *7*, 12273. DOI PubMed PMC
16. Liu, H.; Dao, T. D.; Liu, L.; Meng, X.; Nagao, T.; Ye, J. Light assisted CO_2 reduction with methane over group VIII metals: universality of metal localized surface plasmon resonance in reactant activation. *Appl. Cataly. B. Environ.* **2017**, *209*, 183-9. DOI
17. Yu, X.; Zholobenko, V. L.; Moldovan, S.; et al. Stoichiometric methane conversion to ethane using photochemical looping at ambient

temperature. *Nat. Energy.* **2020**, *5*, 511-9. DOI

18. Liu, Z.; Xu, B.; Jiang, Y. J.; et al. Photocatalytic conversion of methane: current state of the art, challenges, and future perspectives. *ACS. Environ. Au.* **2023**, *3*, 252-76. DOI PubMed PMC
19. Zondag, S. D. A.; Mazzarella, D.; Noël, T. Scale-up of photochemical reactions: transitioning from lab scale to industrial production. *Annu. Rev. Chem. Biomol. Eng.* **2023**, *14*, 283-300. DOI PubMed
20. Lin, X.; Li, J.; Qi, M.; Tang, Z.; Xu, Y. Methane conversion over artificial photocatalysts. *Catal. Commun.* **2021**, *159*, 106346. DOI
21. Wang, Y.; Zhang, H.; Zhang, J.; et al. Low-concentration methane removal: what can we learn from high-concentration methane conversion? *Catal. Sci. Technol.* **2023**, *13*, 6392-408. DOI
22. Wei, J.; Yang, J.; Wen, Z.; Dai, J.; Li, Y.; Yao, B. Efficient photocatalytic oxidation of methane over β-Ga_2O_3/activated carbon composites. *RSC. Adv.* **2017**, *7*, 37508-21. DOI
23. Fan, Y.; Zhou, W.; Qiu, X.; et al. Selective photocatalytic oxidation of methane by quantum-sized bismuth vanadate. *Nat. Sustain.* **2021**, *4*, 509-15. DOI
24. Yu, D.; Jia, Y.; Yang, Z.; et al. Solar photocatalytic oxidation of methane to methanol with water over RuO_x/ZnO/CeO_2 nanorods. *ACS. Sustain. Chem. Eng.* **2022**, *10*, 16-22. DOI
25. Ding, J.; Teng, Z.; Su, X.; et al. Asymmetrically coordinated cobalt single atom on carbon nitride for highly selective photocatalytic oxidation of CH_4 to CH_3OH. *Chem* **2023**, *9*, 1017-35. DOI
26. Zhu, W.; Shen, M.; Fan, G.; et al. Facet-dependent enhancement in the activity of bismuth vanadate microcrystals for the photocatalytic conversion of methane to methanol. *ACS. Appl. Nano. Mater.* **2018**, *1*, 6683-91. DOI
27. Zeng, Y.; Luo, X.; Li, F.; et al. Noble metal-free FeOOH/$Li_{0.1}WO_3$ core-shell nanorods for selective oxidation of methane to methanol with visible-NIR light. *Environ. Sci. Technol.* **2021**, *55*, 7711-20. DOI
28. Wang, Y.; Zhang, J.; Shi, W. X.; et al. W single-atom catalyst for CH_4 photooxidation in water vapor. *Adv. Mater.* **2022**, *34*, 2204448. DOI
29. Zhang, Z.; Zhang, J.; Zhu, Y.; et al. Photo-splitting of water toward hydrogen production and active oxygen species for methane activation to methanol on Co-SrTiO. *Chem. Catal.* **2022**, *2*, 1440-9. DOI
30. Gan, Y.; Huang, M.; Yu, F.; et al. Highly selective photocatalytic methane oxidation to methanol using CO_2 as a soft oxidant. *ACS. Sustain. Chem. Eng.* **2023**, *11*, 5537-46. DOI
31. Song, H.; Meng, X.; Wang, S.; et al. Selective photo-oxidation of methane to methanol with oxygen over dual-cocatalyst-modified titanium dioxide. *ACS. Catal.* **2020**, *10*, 14318-26. DOI
32. Luo, P. P.; Zhou, X. K.; Li, Y.; Lu, T. B. Simultaneously accelerating carrier transfer and enhancing O_2/CH_4 activation via tailoring the oxygen-vacancy-rich surface layer for cocatalyst-free selective photocatalytic CH_4 conversion. *ACS. Appl. Mater. Interfaces.* **2022**, *14*, 21069-78. DOI
33. Luo, L.; Gong, Z.; Xu, Y.; et al. Binary Au-Cu reaction sites decorated ZnO for selective methane oxidation to C1 oxygenates with nearly 100% selectivity at room temperature. *J. Am. Chem. Soc.* **2022**, *144*, 740-50. DOI
34. Luo, L.; Fu, L.; Liu, H.; et al. Synergy of Pd atoms and oxygen vacancies on In_2O_3 for methane conversion under visible light. *Nat. Commun.* **2022**, *13*, 2930. DOI PubMed PMC
35. Jiang, Y.; Li, S.; Wang, S.; et al. Enabling specific photocatalytic methane oxidation by controlling free radical type. *J. Am. Chem. Soc.* **2023**, *145*, 2698-707. DOI
36. Luo, L.; Han, X.; Wang, K.; et al. Nearly 100% selective and visible-light-driven methane conversion to formaldehyde via. single-atom Cu and $W^{\delta+}$. *Nat. Commun.* **2023**, *14*, 2690. DOI PubMed PMC
37. Wu, X.; Zhang, Q.; Li, W.; Qiao, B.; Ma, D.; Wang, S. L. Atomic-scale Pd on 2D titania sheets for selective oxidation of methane to methanol. *ACS. Catal.* **2021**, *11*, 14038-46. DOI
38. Zhu, S.; Li, X.; Pan, Z.; et al. Efficient photooxidation of methane to liquid oxygenates over ZnO nanosheets at atmospheric pressure and near room temperature. *Nano. Lett.* **2021**, *21*, 4122-8. DOI
39. Xie, P.; Ding, J.; Yao, Z.; et al. Oxo dicopper anchored on carbon nitride for selective oxidation of methane. *Nat. Commun.* **2022**, *13*, 1375. DOI PubMed PMC
40. Sun, X.; Chen, X.; Fu, C.; et al. Molecular oxygen enhances H_2O_2 utilization for the photocatalytic conversion of methane to liquid-phase oxygenates. *Nat. Commun.* **2022**, *13*, 6677. DOI PubMed PMC
41. Fang, G.; Wei, F.; Lin, J.; et al. Retrofitting Zr-Oxo nodes of UiO-66 by Ru single atoms to boost methane hydroxylation with nearly total selectivity. *J. Am. Chem. Soc.* **2023**, *145*, 13169-80. DOI
42. Cai, X.; Fang, S.; Hu, Y. H. Unprecedentedly high efficiency for photocatalytic conversion of methane to methanol over Au–Pd/TiO_2 - what is the role of each component in the system? *J. Mater. Chem. A.* **2021**, *9*, 10796-802. DOI
43. Doan, H. A.; Wang, X.; Snurr, R. Q. Computational screening of supported metal oxide nanoclusters for methane activation: insights into homolytic versus heterolytic C-H bond dissociation. *J. Phys. Chem. Lett.* **2023**, *14*, 5018-24. DOI PubMed
44. Chen, Y.; Wang, F.; Huang, Z.; et al. Dual-function reaction center for simultaneous activation of CH_4 and O_2 via oxygen vacancies during direct selective oxidation of CH_4 into CH_3OH. *ACS. Appl. Mater. Interfaces.* **2021**, *13*, 46694-702. DOI
45. Feng, N.; Lin, H.; Song, H.; et al. Efficient and selective photocatalytic CH_4 conversion to CH_3OH with O_2 by controlling overoxidation on TiO_2. *Nat. Commun.* **2021**, *12*, 4652. DOI PubMed PMC
46. Sun, Z.; Wang, C.; Hu, Y. H. Highly selective photocatalytic conversion of methane to liquid oxygenates over silicomolybdic-acid/TiO_2 under mild conditions. *J. Mater. Chem. A.* **2021**, *9*, 1713-9. DOI

47. Zhu, Y.; Chen, S.; Fang, S.; Li, Z.; Wang, C.; Hu, Y. H. Distinct pathways in visible-light driven thermo-photo catalytic methane conversion. *J. Phys. Chem. Lett.* **2021**, *12*, 7459-65. DOI
48. Zhang, W.; Fu, C.; Low, J.; et al. High-performance photocatalytic nonoxidative conversion of methane to ethane and hydrogen by heteroatoms-engineered TiO_2. *Nat. Commun.* **2022**, *13*, 2806. DOI PubMed PMC
49. Wang, X.; Luo, N.; Wang, F. Advances and challenges of photocatalytic methane C-C coupling. *Chin. J. Chem.* **2022**, *40*, 1492-505. DOI
50. Zhang, H.; Sun, P.; Fei, X.; et al. Unusual facet and co-catalyst effects in TiO_2-based photocatalytic coupling of methane. *Nat. Commun.* **2024**, *15*, 4453. DOI PubMed PMC
51. Ma, J.; Mao, K.; Low, J.; et al. Efficient photoelectrochemical conversion of methane into ethylene glycol by WO_3 nanobar arrays. *Angew. Chem. Int. Ed. Engl.* **2021**, *60*, 9357-61. DOI
52. Nie, S.; Wu, L.; Wang, X. Electron-delocalization-stabilized photoelectrocatalytic coupling of methane by NiO-polyoxometalate sub-1 nm heterostructures. *J. Am. Chem. Soc.* **2023**, *145*, 23681-90. DOI PubMed
53. Dong, C.; Marinova, M.; Tayeb, K. B.; et al. Direct photocatalytic synthesis of acetic acid from methane and CO at ambient temperature using water as oxidant. *J. Am. Chem. Soc.* **2023**, *145*, 1185-93. DOI
54. Fang, F.; Sun, X.; Liu, Y.; Huang, W. Water radiocatalysis for selective aqueous-phase methane carboxylation with carbon dioxide into acetic acid at room temperature. *J. Am. Chem. Soc.* **2024**, *146*, 8492-9. DOI
55. Li, X.; Li, C.; Xu, Y.; et al. Efficient hole abstraction for highly selective oxidative coupling of methane by Au-sputtered TiO_2 photocatalysts. *Nat. Energy.* **2023**, *8*, 1013-22. DOI
56. Wang, C.; Li, X.; Ren, Y.; Jiao, H.; Wang, F. R.; Tang, J. Synergy of Ag and AgBr in a pressurized flow reactor for selective photocatalytic oxidative coupling of methane. *ACS. Catal.* **2023**, *13*, 3768-74. DOI PubMed PMC
57. Wang, P.; Shi, R.; Zhao, Y.; et al. Selective photocatalytic oxidative coupling of methane via regulating methyl intermediates over metal/ZnO nanoparticles. *Angew. Chem. Int. Ed. Engl.* **2023**, *62*, e202304301. DOI
58. Wang, Y.; Zhang, Y.; Liu, Y.; Wu, Z. Photocatalytic oxidative coupling of methane to ethane using water and oxygen on Ag_3PO_4-ZnO. *Environ. Sci. Technol.* **2023**, *57*, 11531-40. DOI
59. Wu, S.; Tan, X.; Lei, J.; Chen, H.; Wang, L.; Zhang, J. Ga-doped and Pt-loaded porous TiO_2-SiO_2 for photocatalytic nonoxidative coupling of methane. *J. Am. Chem. Soc.* **2019**, *141*, 6592-600. DOI
60. Chen, Z.; Wu, S.; Ma, J.; et al. Non-oxidative coupling of methane: N-type doping of niobium single atoms in TiO_2-SiO_2 induces electron localization. *Angew. Chem. Int. Ed. Engl.* **2021**, *60*, 11901-9. DOI
61. Singh, S. P.; Yamamoto, A.; Fudo, E.; Tanaka, A.; Kominami, H.; Yoshida, H. A Pd-Bi dual-cocatalyst-loaded gallium oxide photocatalyst for selective and stable nonoxidative coupling of methane. *ACS. Catal.* **2021**, *11*, 13768-81. DOI
62. Zhang, J.; Shen, J.; Li, D.; et al. Efficiently light-driven nonoxidative coupling of methane on Ag/$NaTaO_3$: a case for molecular-level understanding of the coupling mechanism. *ACS. Catal.* **2023**, *13*, 2094-105. DOI
63. Wang, G.; Mu, X.; Li, J.; et al. Light-induced nonoxidative coupling of methane using stable solid solutions. *Angew. Chem. Int. Ed. Engl.* **2021**, *60*, 20760-4. DOI
64. Chen, Z.; Ye, Y.; Feng, X.; et al. High-density frustrated Lewis pairs based on Lamellar Nb_2O_5 for photocatalytic non-oxidative methane coupling. *Nat. Commun.* **2023**, *14*, 2000. DOI PubMed PMC
65. Tang, H.; Chen, Z. A.; Ouyang, C.; et al. Coupling the surface plasmon resonance of WO_{3-x} and Au for enhancing the photocatalytic activity of the nonoxidative methane coupling reaction. *J. Phys. Chem. C.* **2022**, *126*, 20036-48. DOI
66. Zhu, P.; Bian, W.; Liu, B.; et al. Direct conversion of methane to aromatics and hydrogen via a heterogeneous trimetallic synergistic catalyst. *Nat. Commun.* **2024**, *15*, 3280. DOI PubMed PMC
67. Li, D.; Shen, J.; Zhang, J.; et al. Photocatalytic chlorination of methane using alkali chloride solution. *ACS. Catal.* **2022**, *12*, 7004-13. DOI
68. Ma, J.; Zhu, C.; Mao, K.; et al. Sustainable methane utilization technology via photocatalytic halogenation with alkali halides. *Nat. Commun.* **2023**, *14*, 1410. DOI PubMed PMC
69. He, X.; Zhang, L.; Chen, J.; et al. Photo-driven aerobic methane nitration. *Inorg. Chem.* **2023**, *62*, 10343-50. DOI
70. Smith, K. T.; Berritt, S.; González-Moreiras, M.; et al. Catalytic borylation of methane. *Science* **2016**, *351*, 1424-7. DOI
71. Hartwig, J. F. Regioselectivity of the borylation of alkanes and arenes. *Chem. Soc. Rev.* **2011**, *40*, 1992-2002. DOI PubMed
72. Cook, A. K.; Schimler, S. D.; Matzger, A. J.; Sanford, M. S. Catalyst-controlled selectivity in the C-H borylation of methane and ethane. *Science* **2016**, *351*, 1421-4. DOI
73. Shu, C.; Noble, A.; Aggarwal, V. K. Metal-free photoinduced C(sp^3)-H borylation of alkanes. *Nature* **2020**, *586*, 714-9. DOI
74. Zhou, L.; Martirez, J. M. P.; Finzel, J.; et al. Light-driven methane dry reforming with single atomic site antenna-reactor plasmonic photocatalysts. *Nat. Energy.* **2020**, *5*, 61-70. DOI
75. Shoji, S.; Peng, X.; Yamaguchi, A.; et al. Photocatalytic uphill conversion of natural gas beyond the limitation of thermal reaction systems. *Nat. Catal.* **2020**, *3*, 148-53. DOI
76. Khan, A. A.; Tahir, M.; Bafaqeer, A. Constructing a stable 2D Layered Ti_3C_2 MXene cocatalyst-assisted TiO_2/g-C_3N_4/Ti_3C_2 heterojunction for tailoring photocatalytic bireforming of methane under visible light. *Energy. Fuels.* **2020**, *34*, 9810-28. DOI
77. Du, Z.; Pan, F.; Sarnello, E.; et al. Probing the origin of photocatalytic effects in photothermochemical dry reforming of methane on a Pt/CeO_2 catalyst. *J. Phys. Chem. C.* **2021**, *125*, 18684-92. DOI
78. Rao, Z.; Cao, Y.; Huang, Z.; et al. Insights into the nonthermal effects of light in dry reforming of methane to enhance the H_2/CO ratio

near unity over Ni/Ga_2O_3. *ACS. Catal.* **2021**, *11*, 4730-8. DOI

79. Li, Q.; Gao, Y.; Chen, J.; Jia, H. An in situ defect engineering approach for light-driven methane dry reforming over atomically distributed nickel. *Cell. Rep. Phys. Sci.* **2022**, *3*, 101127. DOI
80. Shoji, S.; Bin, M. N. A. S.; Yu, M.; et al. Charge partitioning by intertwined metal-oxide nano-architectural networks for the photocatalytic dry reforming of methane. *Chem. Catal.* **2022**, *2*, 321-9. DOI
81. Low, J.; Long, R.; Xiong, Y. Solar-driven conversion of greenhouse gases toward closing the artificial carbon-cycle loop. *Chem. Catal.* **2022**, *2*, 226-8. DOI
82. Niu, J.; Wang, Y.; Qi, Y.; et al. New mechanism insights into methane steam reforming on Pt/Ni from DFT and experimental kinetic study. *Fuel* **2020**, *266*, 117143. DOI
83. Kaliaguine, S. L.; Shelimov, B. N.; Kazansky, V. B. Reactions of methane and ethane with hole centers O^-. *J. Catal.* **1978**, *55*, 384-93. DOI
84. Villa, K.; Murcia-lópez, S.; Andreu, T.; Morante, J. R. On the role of WO_3 surface hydroxyl groups for the photocatalytic partial oxidation of methane to methanol. *Catal. Commun.* **2015**, *58*, 200-3. DOI
85. Yang, J.; Hao, J.; Wei, J.; Dai, J.; Li, Y. Visible-light-driven selective oxidation of methane to methanol on amorphous FeOOH coupled m-WO_3. *Fuel* **2020**, *266*, 117104. DOI
86. Li, N.; Li, Y.; Jiang, R.; Zhou, J.; Liu, M. Photocatalytic coupling of methane and CO_2 into C_2-hydrocarbons over Zn doped g-C_3N_4 catalysts. *Appl. Surf. Sci.* **2019**, *498*, 143861. DOI
87. Linic, S.; Christopher, P.; Ingram, D. B. Plasmonic-metal nanostructures for efficient conversion of solar to chemical energy. *Nat. Mater.* **2011**, *10*, 911-21. DOI PubMed
88. García-diéguez, M.; Pieta, I.; Herrera, M.; Larrubia, M.; Alemany, L. Nanostructured Pt- and Ni-based catalysts for CO_2-reforming of methane. *J. Catal.* **2010**, *270*, 136-45. DOI
89. Christopher, P.; Xin, H.; Linic, S. Visible-light-enhanced catalytic oxidation reactions on plasmonic silver nanostructures. *Nat. Chem.* **2011**, *3*, 467-72. DOI PubMed
90. Schuller, J. A.; Barnard, E. S.; Cai, W.; Jun, Y. C.; White, J. S.; Brongersma, M. L. Plasmonics for extreme light concentration and manipulation. *Nat. Mater.* **2010**, *9*, 193-204. DOI PubMed
91. Darvas, F.; Hessel, V.; Dorman, G. Volume 1 Flow chemistry - Fundamentals. Berlin, Boston: De Gruyter, 2014. DOI

Yizhe Xiong is currently an undergraduate student at the College of Chemistry, Beijing Institute of Technology. His research interests center on the design and mechanisms of photocatalytic methane conversion.

Jiahong Liu is a Ph.D. candidate at the Advanced Research Institute of Multidisciplinary Sciences, Beijing Institute of Technology, supervised by Professor Yiou Wang. He earned his bachelor's degree from South China University of Technology. His doctoral research focuses on the performance and mechanisms of light-driven radical-based reactions.

Prof. Yiou Wang is a Principal Investigator at the Advanced Research Institute of Multidisciplinary Sciences, at Beijing Institute of Technology. He received his bachelor's degree from Peking University and obtained his Ph.D. from University College London. Following this, he served as an Alexander von Humboldt Fellow at Ludwig-Maximilians-Universität München, Germany, before joining Beijing Institute of Technology. His research is dedicated to the synergistic regulation of charge carrier dynamics and surface reactions in photocatalysis, with a particular emphasis on mechanism studies using optical spectroscopies.